Stochastic cascade models of two and three dimensional turbulence

Jes Ravnbøl

December 1, 2010

Abstract

A pair of simple stochastic cascade models of 2 and 3 dimensional turbulence are proposed and investigated. The two models are similar in structure, but differ with respect to their conserved integrals. The 2D model conserves energy and enstrophy like quantities in the unforced, inviscid limit, where as the 3D model conserves energy and helicity like quantities in the unforced, inviscid limit.
It is shown from numerical simulations that the 3D model has an inertial range with a direct cascade of energy, and an energy spectrum displaying kolmogorov scaling.
Similarly it is shown from simulations, that the 2D model has two inertial ranges and two cascades: A direct cascade of enstropy and an inverse cascade of energy. The energy spectrum of the 2D model also shows Kolmogorov scalings for both the energy and enstrophy cascades.
Neither the 2D nor the 3D model show intermittency corrections to the scaling exponents of the structure functions.

Contents

Figure 1: Turbulence in a river

1 Introduction

Turbulence is the wildly erratic and time-dependent flow that occurs in a fluid under certain conditions. It is observed under such different circumstances as the flow of fluids in pipes, the stirring of a bathtub, water passing a rock in a river and the flow in the atmosphere. A picture of turbulence in a river is shown in figure 1.

A wide range of fluids, including water and air, are believed to behave according to the incompressible Navier-Stokes equations(NSE's) (4), which have been known for about 200 years. Implicitely, the phenomenon of turbulence is believed to be a feature of the NSE's.
However, no general solution is known for these partial, non-linear differential equations; only steady-state and very simple time dependent solutions [*Wang*, 1990]. In general, solutions are chaotic, i.e. a perturbation of the initial conditions grows exponentially.

It goes without saying that understanding and predicting the behaviour of fluids is of immense importance for engineering purposes, as well as of great academic interest. Fluid dynamical problems are hard even without the presence of turbulence. Much effort has gone into finding steady state(i.e. time independent) solutions of the NSE's and tailor expanding the equations around these solutions, to see how small perturbations behave.
However, a turbulent flow is far from time independent. It has rapid variations in velocity and pressure over space and time. Such a solution, surely, can not be understood by linearizing the NSE's around a steady state solution.
In regimes where viscous damping is either negligible or dominant, the NSE's can be ap-

proximated by the Euler equations or the Stokes equations respectively. These equations are easier to deal with, all though the Euler equations are still not integrable. However, one can not hope to describe turbulent flow by looking at the approximative Stokes or Euler equations. Stokes equations describes the limit where viscous forces dominate, and turbulence is characterised by the opposite limit of high Reynolds numbers(see equation (8)). As for Eulers equations, they completely leave out dissipation. This does not allow for energy to be dissipated at small scales, a central part of turbulence(See section 2.2). Therefore, one has to look at the full NSE's, when dealing with turbulence.
This seems an impossible task, given the chaotic nature of the solutions. However, it turns out that the flow of turbulent fluids share some statistical features, whether you are looking at the stirring of a bathtub or the flow of air past a speeding car. Certain statistical aspects of turbulent flows seem to be universal.

The phenomenological picture of turbulence in a 3 dimensional(3D) fluid, is due to Richardson, and is described in section 2.2. In the Richardson picture of turbulence, the flow consists of eddies of all sizes. The large eddies break up in to smaller eddies, and this is repeated until the eddies become so small, that they are dissipated because of viscosity. In this way, energy that is put in to the fluid on large scales, is cascaded to small scales where it is dissipated.

The situation is quite different for turbulence in a 2 dimensional(2D) fluid. Here, it is generally assumed that energy is cascaded to larger scales and is eventually dissipated by friction with the boundaries, and that a second conserved integral, called enstrophy, is cascaded to smaller scales where it is dissipated by viscosity. This idea of a double cascade is attributed to R. H. Kraichnan.

The most successful theory of turbulence is Kolmogorovs scaling theory from 1941, described in section 2.2.3. The theory predicts statistical features of a turbulent flow. Specifically, it predicts the scaling exponents of the energy spectrum and the so called structure functions, by a universality argument. In spite of the success of Kolmogorovs theory, there are many aspects of turbulence that are still not understood. The theory has no connection to the NSE's and experiments show corrections to the scaling exponents that it predicts.

The field of turbulence research is huge, and many different approaches has been taken to gain insight into the problem. One such rout has been to investigate simpler, phenomenological models that share some of the characteristics of the NSE's. The hope is that understanding these models will lead to a better understanding of the fundamental mechanisms driving turbulence.
An example of such a phenomenological model, that has drawn considerable interest, is the GOY shell model[*Yamada and Ohkitani*, 1987]. The model has a structure similar to the NSE's in spectral space, but a highly reduced number of degrees of freedom, and is therefore easier to investigate on a computer.

The models presented in this thesis are, like the GOY shell model, phenomenological models. The aim has been to develop simple stochastic cascade models of 2 and 3 dimensional turbulence, that show the Richardson cascade(3D) and the Kraichnan double cascade(2D), and have energy spectrums that scale according to K41 theory.

The models have been constructed to have a structure similar to the NSE's in spectral

space, and conserved integrals that resemble the ones of the NSE's for 2 and 3 dimensional fluids respectively.

The outline of the thesis is as follows:
In section 2 a short account of some relevant theory is presented. Section 2.1, 2.2 and 2.3 give brief introductions to the Navier-Stoke equations, the Richardson cascade, the Kraichnan double cascade and Kolmogorovs 1941 theory. Section 2.4 and 2.5 review stochastic processes and time series analysis.
In section 3, the two models are introduced and their dynamics discussed.
Finally, in section 4, results from numerical simulations of the models are presented.

2 Theory

In order to provide a background for the models to be introduced in section 3, the following sections will give short reviews of fluid dynamics, turbulence, stochastic processes, and time series analysis.

2.1 The Navier-Stokes equations

This section reviews elements of fluid dynamics that are central to turbulence and the models investigated in the thesis.
The Navier-Stokes equations for an incompressible fluid are formulated and recast in spectral space, and in the form of the vorticity equations. Conserved integrals of the Navier-Stokes equations in two and three dimensions are discussed and, lastly, the energy and enstrophy flux are definded.

In fluid dynamics, it is assumed that a fluid can be described as a continuum. The microscopic details of the fluid, the position and velocity of single atoms or molecules, is ignored, and microscopic properties only couple to the description through material constants, such as density and viscosity. The enormous number of degrees of freedom present in the microscopic description is replaced by a set of fields that represent averages over the microscopic details. This is a good approximation if the mean free path of a particle in the fluid is small compared to a characteristic length scale of the flow(the ratio between the two is called the Knudsen number).
If the fluid is electrically neutral, it can be described by the following fields:

- The velocity field: $\mathbf{v}(\mathbf{x}, t)$
- The density field: $\rho(\mathbf{x}, t)$
- The stress tensor field: $\sigma(\mathbf{x}, t)$

The velocity field is the velocity of the fluid at $(\mathbf{x}, t)$. The density field is the local density, such that the mass of a volume dV at $(\mathbf{x}, t)$ is $\rho(\mathbf{x}, t)dV$.
Finally, the stress tensor describes the surface forces acting on surfaces, real or imaginary, in the fluid. If a surface has normal vector $\hat{\mathbf{n}}$, at $\mathbf{x}$, the force on an infinitesimal surface area dA, at this position, along the i'th unit vector is(See figure 2)

$$\sigma_{ij}(\mathbf{x}, t)\hat{n}_j dA$$

where an index notation, described in appendix A.1, has been used. Notice that the surface forces on all surfaces having the same normal vector $\hat{\mathbf{n}}$ at $\mathbf{x}$ are the same.

The theory sets up a set of coupled partial differential equations for the fields listed above, on the basis of Newtons second law of motion.
If one considers the forces acting on a volume of fluid(with no external force fields, such as gravity), and uses Gauss' theorem of integration, Newtons second law of motion can be expressed as

$$\rho(\mathbf{x}, t)\big(\partial_t v_i(\mathbf{x}, t) + v_j(\mathbf{x}, t)\partial_j v_i(\mathbf{x}, t)\big) = \partial_j \sigma_{ij}(\mathbf{x}, t) \tag{1}$$

For a derivation of this equation, see appendix A.2
A wide variety of fluids(e.g. water and air) are belived to have a stress tensor of the form

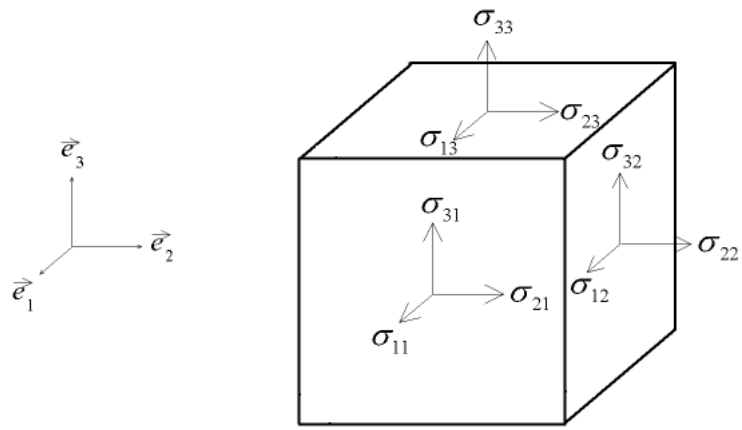

Figure 2: The figure shows the nine components of the stress tensor, as they relate to the forces on the sides of a cube with unit area sides, that have normal vectors equal to the unit vectors. For such a cube, the forces acting on the surfaces, are simply the components of the stress tensor

$$\sigma_{ij}(\mathbf{x},t) = -\delta_{ij}p(\mathbf{x},t) + \eta\big(\partial_j v_i(\mathbf{x},t) + \partial_i v_j(\mathbf{x},t)\big) \tag{2}$$

where η is a material constant called the dynamical viscosity of the fluid. Fluids that obey equation (2) are referred to as newtonian fluids.

A simplification of the equations of motion, can be achived by considering the flow as incompressible. This requires the velocity field to have zero divergence:

$$\nabla \cdot \mathbf{v} = 0 \tag{3}$$

Combining the form of the stress tensor for a newtonian fluid, (2), the incompressibility recuirement, (3), and newtons second law of motion, (1), we arrive at the Navier-Stokes equations for an incompressible, Newtonian fluid:

$$\rho\Big(\partial_t \mathbf{v} + \big(\mathbf{v}\cdot\nabla\big)\mathbf{v}\Big) = -\nabla p + \eta\triangle\mathbf{v} \tag{4}$$

It can be shown from conservation of mass, that the material derivative of the density for an incompressible fluid is zero. This means that the density is constant when following a fluid particle.
If it is assumed that the density is everywhere the same, one can introduce the kinematic viscosity $\nu = \eta/\rho$, and rewrite the NSE's as

$$\partial_t \mathbf{v} + \big(\mathbf{v}\cdot\nabla\big)\mathbf{v} = -\frac{\nabla p}{\rho} + \nu\triangle\mathbf{v} \tag{5}$$

Together with the incompressibility requirement (3), this vector equation forms a closed set of 4 equations with 4 scalar fields $\{p, v_x, v_y, v_z\}$, that fully describes the evolution of the netonian fluid.
Equation (4) can be seen as Newtons second law for a fluid particle, in a coordinate system following the path of the fluid particle. The two terms on the left hand side of the equation are called the material derivative of the momentum per volume. They express the rate of change in momentum per volume, when following a fluid particle at $(\mathbf{x},t)$. The first term is the change in momentum due to a change in the velocity field over time. The second term is the change in momentum that comes about because the fluid particle

moves in the velocity field, and is fittingly called the advective term. It will be present even in a steady state velocity field.
The two terms on the right hand side of the equation represent the contact forces per volume on the fluid particle. The first term, the gradient of the pressure, describes the effect of forces acting normal on the surfaces of the fluid particle. The second term describes the shear stress forces on the surface of the fluid particle. The shear forces are zero when the fluid is at rest.

The NSE's can be non-dimensionalised by introducing a characteristic velocity, V, and lenght, L. Defining new, dimensionless fields:

$$\mathbf{v} = V\tilde{\mathbf{v}}, \;\; \mathbf{x} = L\tilde{\mathbf{x}}, \;\; t = (L/V)\tilde{t}, \;\; (p/\rho) = V^2\tilde{p}$$

the NSE's become

$$\partial_t\tilde{\mathbf{v}} + \big(\tilde{\mathbf{v}}\cdot\nabla\big)\tilde{\mathbf{v}} = -\nabla\tilde{p} + \frac{1}{Re}\triangle\tilde{\mathbf{v}} \tag{6}$$

$$\nabla\cdot\tilde{\mathbf{v}} = 0 \tag{7}$$

Where we have introduced a dimensionless number, characteristic of the flow, called the Reynolds number

$$Re = \frac{VL}{\nu} \tag{8}$$

The non-dimensional NSE's (6) and (7) reveal an important property of incompressible fluids, called the similarity principle: That flow on large scales are governed by the same dynamics as flow on small scales. If the geometry and Reynolds number are the same, then the solutions of the NSE's are similar, only rescaled. An example of a possible situation is illustrated in figure 3. It shows a cross section of a uniform flow impending on a cylinder. The characteristic length is the diameter of the cylinder, and the characteristic velocity is the uniform velocity of the incoming flow, far away from the cylinder. If the diameter of the cylinder and the velocity of the incoming flow are changed, while keeping the Reynolds number constant, the flow around the cylinder will be the same, only rescaled.
The Reynolds number also serves as a measure of the relative importance of the acceleration and the viscous forces per mass. It is the ratio of the characteristic acceleration V^2/L and the characteristic viscous force per mass $\nu V/L^2$. Turbulent flow, is signified by high Reynolds numbers, as will be discussed further in section 2.2.

2.1.1 The vorticity equations

For many purposes it is useful to look at the curl of the velocity field, the so called vorticity, that describes the local rotation of the velocity field.

$$\boldsymbol{\omega} = \nabla\times\mathbf{v} \tag{9}$$

The evolution of the vorticity is governed by the vorticity equation, which can be found by taking the curl of the NSE's (6).

$$\nabla\times\big(\partial_t\mathbf{v}\big) + \nabla\times\big(\mathbf{v}\cdot\nabla\big)\mathbf{v} = -\nabla\times\nabla p + \frac{1}{Re}\nabla\times\triangle\mathbf{v} \tag{10}$$

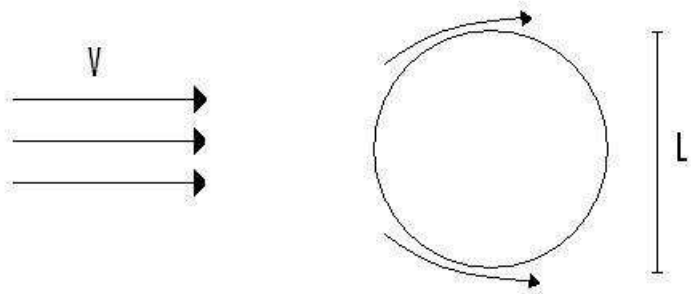

Figure 3: The figure shows the flow past a cylinder. The diameter of the cylinder is L and the velocity far from the cylinder is uniform with magnitude V

Using the fact that differential operators commute, that the curl of a gradient is zero and the incompressibility of the fluid, we get(see [*Ditlevsen*, 2004, p. 309] for a full derivation)

$$\partial_t \boldsymbol{\omega} + \big(\mathbf{v} \cdot \nabla\big)\boldsymbol{\omega} = \big(\boldsymbol{\omega} \cdot \nabla\big)\mathbf{v} + \frac{1}{Re}\triangle\boldsymbol{\omega} \tag{11}$$

The left hand side is the material derivative of the vorticity. The right hand side consists of two terms: The first one, a non linear term, called the bending and stretching term. It is the term that creates vorticity. The second term, a linear term, responsible for the dissipation of vorticity.
The vorticity equations (11) and (9) are a closed set of 6 equations with 6 scalar fields: $\{v_x, v_y, v_z, \omega_x, \omega_y, \omega_z\}$. The pressure field has been eliminated from the original NSE's, at the expense of introducing 3 new scalar fields.

2.1.2 Conserved integrals

For a three dimensional flow, the NSE's have two conserved integrals in the inviscid limit, $\nu \to 0$, the total energy and helicity:

$$E = \int_V \mathrm{d}\mathbf{x}\ E(\mathbf{x}, t) = \frac{1}{2}\int_V \mathrm{d}\mathbf{x}\ \|\mathbf{v}\|^2 \tag{12}$$

$$H = \int_V \mathrm{d}\mathbf{x}\ H(\mathbf{x}, t) = \frac{1}{2}\int_V \mathrm{d}\mathbf{x}\ \mathbf{v} \cdot \boldsymbol{\omega} \tag{13}$$

Where the integration is over the volume, V, of the fluid, and

$$E(\mathbf{x}, t) = \frac{1}{2}\|v(\mathbf{x}, t)\|^2$$

$$H(\mathbf{x}, t) = \frac{1}{2}\mathbf{v}(\mathbf{x}, t) \cdot \boldsymbol{\omega}(\mathbf{x}, t)$$

are the local energy and helicity densities. Notice, that the energy is a strictly positive quantity, whereas the helicity can take on negative values.

To show that the two integrals (12) and (13) are conserved in the inviscid limit, one can multiply the Navier-Stokes equations or the vorticity equations by the velocity field and integrate over the volume filled by the fluid. Assuming that the velocity and pressure field vanishes at the boundaries one gets following equations for the change in kinetic energy and helicity(see [*Frisch*, 1995, p. 14]):

$$\frac{dE}{dt} = -\nu \int_V \mathrm{d}\mathbf{x}\ |\boldsymbol{\omega}|^2 + F \tag{14}$$

$$\frac{dH}{dt} = -\nu \int_V \mathrm{d}\mathbf{x}\ \boldsymbol{\omega} \cdot \nabla \times \boldsymbol{\omega} + H_F \tag{15}$$

Where we have introduced the rates of energy and helicity put in to the system by forcing(i.e. stirring), F and H_F. Since the helicity is not a strictly positive quantity, the helicity input need not be positive. The NSE's are diffusive, because of the first term on the right hand side of equation (14). However, we see that in the unforced, inviscid limit($F = H_F = \nu = 0$), both the total energy and helicity are conserved.

In two dimensional flow, the Navier-Stokes equations have an extra conserved integral, the enstrophy. The local enstrophy density is

$$Z(\mathbf{x}, t) = \frac{1}{2}\|\boldsymbol{\omega}(\mathbf{x}, \boldsymbol{t})\|^2$$

So the total enstrophy is:

$$Z = \frac{1}{2}\int_V \mathrm{d}\mathbf{x}\ \|\boldsymbol{\omega}\|^2 \tag{16}$$

The enstrophy is, in fact, not only a conserved integral, but a passively advected scalar field. This may be realized by looking at the vorticity equation (11), for a two dimensional fluid. The local vorticity will always be perpendicular to the plane of the flow, and can be represented by a scalar field. The stretching and bending term, $\big(\boldsymbol{\omega} \cdot \nabla\big)\mathbf{v}$, which produces enstrophy, is zero, since the velocity and vorticity is everywhere perpendicular. Since the vorticity is passively advected, the total vorticity squared, is trivially a conserved integral in the invicid limit.
The enstrophy is a positive definite quantity like the energy, which plays an important role in 2D turbulence.

2.1.3 The spectral Navier-Stokes equations

Another useful reformulation of the NSE's comes from looking at the velocity and pressure field in spectral space. Assuming that these fields are confined to a box of sides $L_x L_y L_z$ and volume $V = L_x L_y L_z$, they may be expanded in the basis, $\{e^{i\mathbf{k}\cdot\mathbf{x}} \mid k \in (\frac{2\pi}{L_x}, \frac{2\pi}{L_x}, \frac{2\pi}{L_x}) \times \mathbb{Z}^3\}$, of exponential functions that are periodic over the box.

$$v_i(\mathbf{x}, t) = \sum_{\mathbf{k}} \tilde{v}_{i,\mathbf{k}}(t) e^{i\mathbf{k}\cdot\mathbf{x}}, \qquad \mathbf{k} \in (\frac{2\pi}{L_x}, \frac{2\pi}{L_x}, \frac{2\pi}{L_x}) \times \mathbb{Z}^3 \tag{17}$$

$$p(\mathbf{x}, t) = \sum_{\mathbf{k}} \tilde{p}_{i,\mathbf{k}}(t) e^{i\mathbf{k}\cdot\mathbf{x}}, \qquad \mathbf{k} \in (\frac{2\pi}{L_x}, \frac{2\pi}{L_x}, \frac{2\pi}{L_x}) \times \mathbb{Z}^3 \tag{18}$$

where the coefficients of expansion, the fourier coefficients, are

$$\tilde{v}_{i,\mathbf{k}}(t) = \frac{1}{V}\int_V \mathrm{d}\mathbf{x}\ v_i(\mathbf{x}, t) e^{i\mathbf{k}\cdot\mathbf{x}} \tag{19}$$

$$\tilde{p}_{\mathbf{k}}(t) = \frac{1}{V}\int_V \mathrm{d}\mathbf{x}\ p(\mathbf{x}, t) e^{i\mathbf{k}\cdot\mathbf{x}} \tag{20}$$

By taking the fourier transform of both sides of the NSE's (5) and manipulating the expressions(see [*Ditlevsen*, 2004, p. 13]) we get the spectral Navier-Stokes equations

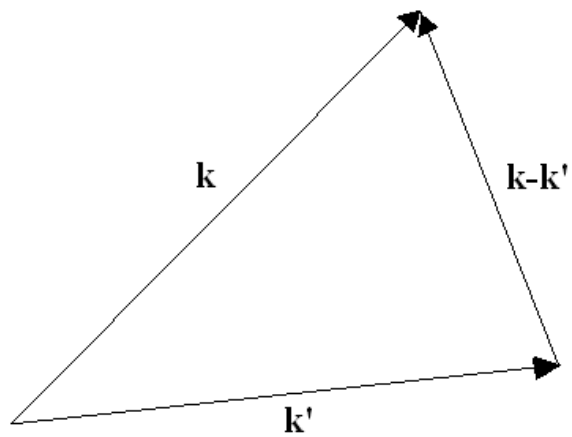

Figure 4: Three wave vectors involved in a triad interaction

$$\frac{d}{dt}\tilde{v}_{i,\mathbf{k}} = -ik_j \sum_{\mathbf{k}'} \left(\delta_{il} - \frac{k'_l k_i}{k^2}\right)\tilde{v}_{j,\mathbf{k}'}\tilde{v}_{l,\mathbf{k}-\mathbf{k}'} - \nu k^2 \tilde{v}_{i,\mathbf{k}} = \sum_{\mathbf{k}'} I(\mathbf{k},\mathbf{k}')\tilde{v}_{j,\mathbf{k}'}\tilde{v}_{l,\mathbf{k}-\mathbf{k}'} - \nu k^2 \tilde{v}_{i,\mathbf{k}} \quad (21)$$

Where we have introduced $I(\mathbf{k},\mathbf{k}') = -ik_j\left(\delta_{il} - \frac{k'_l k_i}{k^2}\right)$. The NSE's, which is a set of partial differential equations, have been transformed in to an infinite hirachy of ordinary differential equations for the fourier coeficients of the velocity field. Using the incompressibility requirement (3), the pressure has been eliminated from the equations.
It is interesting to look at the structure of the spectral Navier-Stokes equations, especially the quadratic, non-linear terms, responsible for the transfer of energy between different length scales in the fluid. We see that velocity wave modes couple in so called triad interactions. The fourier component with wave vector $\mathbf{k}$ couple to pairs of other fourier components, $\mathbf{k}'$ and $\mathbf{k}-\mathbf{k}'$ in such a way that the wave vectors add up to zero. Figure 4 shows three such vectors, and at the same time explains the name "triad interactions". The strenght of a specific triad interaction, is the quantity $I(\mathbf{k},\mathbf{k}')$

From the fourier components of the velocity field one can construct the spectral energy:

$$E_{\mathbf{k}}(t) = \frac{1}{2}|\tilde{\boldsymbol{v}}_{\mathbf{k}}(t)|^2 \quad (22)$$

This is not the fouriertransform of the energy density, but one half the squared length of the fourier transform of the velocity field.
Parcevals theorem tells us that the total energy can be written as

$$E = \frac{1}{2}\int_V \mathrm{d}\mathbf{x}\ \|\mathbf{v}\|^2 = \frac{1}{2}\sum_{\mathbf{k}} |\tilde{\boldsymbol{v}}_{\mathbf{k}}(t)|^2 = \sum_{\mathbf{k}} E_{\mathbf{k}}(t), \qquad \mathbf{k} \in \left(\frac{2\pi}{L_x}, \frac{2\pi}{L_x}, \frac{2\pi}{L_x}\right) \times \mathbb{Z}^3 \quad (23)$$

Talking the scalar product between the spectral Navier-Stokes equations (21) and $\frac{1}{2}\tilde{\mathbf{v}}_{-\mathbf{k}}$ and adding the complex conjugate, we get an equation for the evolution of the spectral energy.

$$\frac{d}{dt}E_{\mathbf{k}} = \frac{1}{2}\sum_{\mathbf{k}'} I(\mathbf{k},\mathbf{k}')\tilde{v}_{j,\mathbf{k}'}\tilde{v}_{l,\mathbf{k}-\mathbf{k}'}\tilde{v}_{i,-\mathbf{k}} - \frac{\nu}{2}k^2 E_{\mathbf{k}} + c.c. \quad (24)$$

Where c.c. means the complex conjugate of the two first terms. The models investigated in this thesis, are constructed to have a structure that resembles this differential equation for the spectral energy density, in its nonlinear triad interactions, $\tilde{v}_{j,\mathbf{k}'}\tilde{v}_{l,\mathbf{k}-\mathbf{k}'}\tilde{v}_{i,-\mathbf{k}}$.

If one introduces the fourier transform of the vorticity, a spectral enstrophy can be constructed in exactly the same way as the spectral energy density

$$Z_{\mathbf{k}}(t) = \frac{1}{2}|\tilde{\boldsymbol{\omega}}_{\mathbf{k}}(t)|^2 \tag{25}$$

Using the incompressibility of the fluid it can be shown that(see [*Ditlevsen*, 2004, p. 313])

$$Z_{\mathbf{k}}(t) = k^2 E_{\mathbf{k}}(t) \tag{26}$$

Again, Parcevals theorem can be used to write the total enstrophy as

$$Z = \sum_{\mathbf{k}} Z_{\mathbf{k}} = \sum_{\mathbf{k}} k^2 E_{\mathbf{k}}(t), \qquad \mathbf{k} \in (\frac{2\pi}{L_x}, \frac{2\pi}{L_x}, \frac{2\pi}{L_x}) \times \mathbb{Z}^3 \tag{27}$$

When the volume V of the fluid grows, the spacing between the Fourier modes in k-space becomes smaller. In the limit $V \to \infty$, Fourier space becomes continuous and the spectral energy and enstrophy become densities.

2.1.4 The energy spectrum, and the energy and enstrophy flux

In equation (22) and (25) the spectral energy and enstrophy were defined. These give the energy and enstrophy present in wave modes with wave vector $\mathbf{k}$. Often it is more useful to look at the energy and enstrophy in wave modes with a certain length $k = \|\mathbf{k}\|$, corresponding to a sphere in k-space of radius k. This is called the energy spectrum. In the limit of continuous k-space, the energy spectrum can be defined by the surface integral

$$E(k,t) = \oint_{S(k)} E(\mathbf{k},t)\ dS(k) \tag{28}$$

Where S(k) is a sphere of radius k. $E(k,t)dk$ gives the kinetic energy present in Fourier modes with wave vectors that has lengths in the interval $[k, k+dk]$. The kinetic energy on length scales smaller than than $1/K$ can be expressed by the cumulative energy spectrum:

$$\mathcal{E}(k,t) = \int_0^k dk'\ \ E(k',t) \tag{29}$$

In a completely analogous way, the enstrophy spectrum can be defined as

$$Z(k,t) = \oint_{S(k)} Z(\mathbf{k},t)\ dS(k) = \oint_{S(k)} k^2 E(\mathbf{k},t) dS(k) = k^2 E(k,t) \tag{30}$$

And the cumulative enstrophy spectrum as

$$\mathcal{Z}(k,t) = \int_0^k dk'\ \ Z(k',t) = \int_0^k dk'\ \ k^2 E(k',t) \tag{31}$$

An alternative definition of the energy and enstrophy spectrum, in terms of high and low pass filters is given in [*Frisch*, 1995, p. 21].

In turbulence, one is often interested in the transfer of energy between different length scales in the fluid. The cumulative energy spectrum, that expresses the kinetic energy on

length scales smaller than $1/K$, changes for 3 reasons: Dissipation of energy, transfer of energy to length scales greater than $1/K$ and forcing(i.e energy input). The transfer of energy to larger length scales is what is referred to as the energy flux. It is solely due the the non linear terms in the NSE's, and can be written as

$$\Pi_K^E(t) = \partial_t|_{N.L}\mathcal{E}(k,t) \tag{32}$$

where the derivative $\partial_t|_{N.L}$ denotes the change due to the non linear terms in the NSE's. An explicit expression for the energy flux, can be obtained from the SNSE's. The interested reader may consult [*Frisch*, 1995, p. 21] or [*Ditlevsen*, 2004, p. 16].

In the same manner, the enstrophy flux can be defined as

$$\Pi_K^Z(t) = \partial_t|_{N.L}\mathcal{Z}(k,t) \tag{33}$$

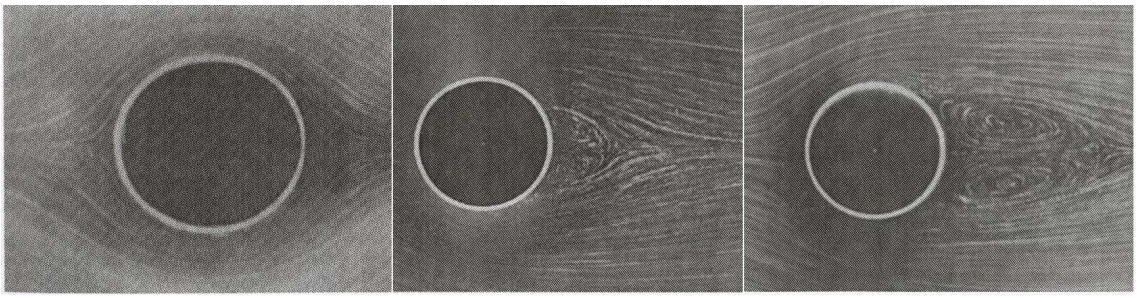

Figure 5: The figure shows 3 different flows past a cylinder. The flow in the left figure has a Reynolds number $Re = 0.16$, the flow in the middle figure has $Re = 13.1$ and the flow in the right figure has $Re = 26$. The images have been taken from [*Frisch*, 1995, p. 3,5]

2.2 Turbulence in 3D

This section will review some of the theory and phenomenology of turbulence in a 3 dimensional fluid. Richardsons phenomenological picture of turbulence is described, the statistical description of a turbulent fluid is introduced and Kolomogorovs famous 1941 theory(K41) is reviewed. Finally, experimental investigations of turbulence and the deviations from K41 theory is briefly touched upon.

To motivate the discussion of turbulence, we look at the 3 situations in figure 5, that show different flows past a cylinder. Far from the cylinder, the flows are laminar with a uniform velocity field. The Reynolds number is different for the 3 flows and is determined from the uniform velocity field far from the cylinder, the diameter of the cylinder and the kinematic viscosity of the fluid(see equation 8). For a low Reynolds number(left figure) the flow behind the cylinder is laminar. As the Reynolds number is increased(middle figure), turbulence sets in. Finally, when the Reynolds number becomes large enough(right figure), the turbulence becomes fully developed. The term fully developed turbulence has a statistical meaning that will be described later.
Regardless of the specific flow(be it the flow in a pipe or the flow past a cylinder), turbulence is always characterized by high Reynolds numbers. The actual value of the Reynolds number, for which the flow crosses over from laminar to turbulent, is specific to the geometry of the situation.

2.2.1 The Richardson cascade and forced steady state

The phenomenological picture of turbulence in a 3D fluid is due to Richardson. In the Richardson picture of turbulence, the flow consists of eddies of all sizes. The large eddies break up in to smaller eddies, and this is repeated until the eddies become so small, that they are dissipated by viscosity. When an eddy breaks in to smaller eddies, its kinetic energy is transferred to the smaller eddies, and in this way, energy that is put in to the fluid on large length scales, is cascaded to small length scales, where it is dissipated by viscosity. An illustration is shown in figure 6.

In the following, we consider a situation where the turbulent flow has reached a steady state, in which the energy input, due to forcing on large scales, is balanced by the dissipation of energy on small scales. This is referred to as forced steady state turbulence.

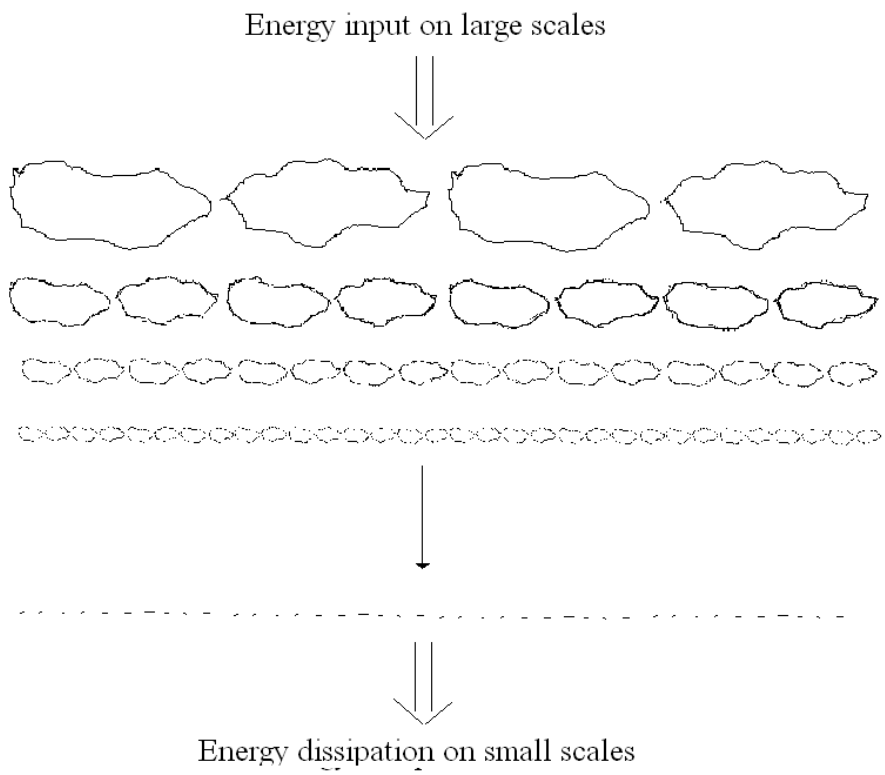

Figure 6: The figure shows the idea of the Richardson cascade. Energy is put in to the fluid at large scales and cascaded to small scales, where it is dissipated

2.2.2 Statistical description of fully developed turbulence

As mentioned in the introduction, a turbulent flow has rapid variations in the velocity and pressure fields. Despite the chaotic nature of such a turbulent flow, it turns out to exhibit some predictability in a statistical sense. In the forced steady state, described above, the velocity field of the fluid is in equilibrium in a statistical sense. That is, the statistical properties of the velocity field are constant in time(They are not, however, described by equilibrium statistical mechanics).
An obvious question is: What is meant by the statistical properties of a velocity field that is governed by a deterministic differential equation?
In order to view the velocity field as a stochastic function, one imagines an ensemble of systems drawn from some distribution of initial conditions for the velocity field. In this way, the velocity field at later times will have a probability distribution that can in principle be found from the NSE's and will be time dependent in general(see [*Ditlevsen*, 2004, p. 146]).
However, for forced, steady state turbulence, it is generally assumed, that when the Reynolds number becomes high enough, the stochastic velocity field becomes stationary, meaning that it's probability distribution is time independent(see section 2.4.3 on stationary stochastic processes). It is also assumed, that the dynamics are ergodic, so that ensemble averages can be calculated as time averages(see [*Frisch*, 1995, p. 36] or [*Ditlevsen*, 2004, p. 12])

$$\Big\langle f(\mathbf{v}(\mathbf{x}))\Big\rangle_{ensemble} = \lim_{T\to+\infty}\frac{1}{T}\int_{\tau}^{\tau+T}\mathrm{d}t\ f(\mathbf{v}(\mathbf{x},t)) \tag{34}$$

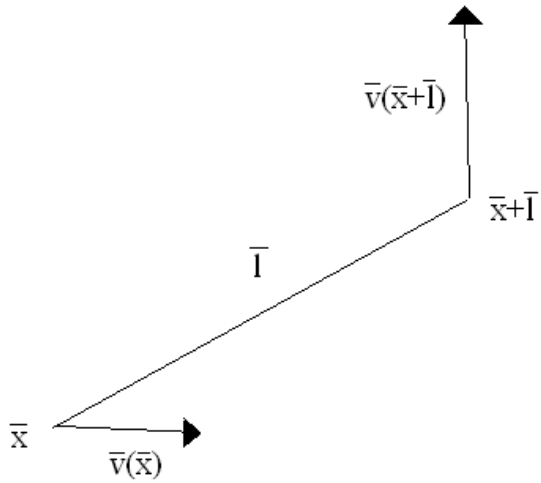

Figure 7: The figure illustrates the components involved in the structure functions

This implies, that the distribution of initial conditions is forgotten by the dynamics(Something that would obviously not be true in a laminar flow). The stationarity and ergodicity of the velocity field, allows researchers to measure the velocity field at different times, and calculate the ensemble averages as time averages.

When studying the statistical properties of the velocity field, one looks at velocity increments

$$\delta\mathbf{v}(\mathbf{x},\mathbf{l},t) = \mathbf{v}(\mathbf{x}+\mathbf{l},t) - \mathbf{v}(\mathbf{x},t) \tag{35}$$

The statistical properties of the velocity increments can be investigated through the structure functions

$$S_p(\mathbf{x},\mathbf{l}) = \left\langle \|\mathbf{v}(\mathbf{x}+\mathbf{l},t) - \mathbf{v}(\mathbf{x},t)\|^p \right\rangle \tag{36}$$

where p is the order of the structure function and the reference to the ensemble of initial conditions has been dropped in the expectation value. The structure functions give the mean length of the velocity difference in two points $\mathbf{x}$ and $\mathbf{x}+\mathbf{l}$, to some power p. They have no time dependence because we are looking at situations where the velocity field is stationary.

2.2.3 K41 scaling theory

In his famous paper from 1941, Kolmogorov proposed that the statistical properties of a turbulent flow are homogeneous, isotropic and scale invariant. His scaling theory, called K41 theory, is based on the following assumptions:

- When the Reynolds number becomes sufficiently large, the statistical properties of velocity increments on length scales much smaller than the scale of the system, L_0, will be isotropic and homogeneous

- There is a range of length scales, $L_0 >> l >> \eta$, called the inertial range, where the statistical properties of velocity increments are universally determined by the length scale, l, and the average rate of energy dissipation per unit mass, $\bar{\epsilon}$.

The first assumption states that at length scales much smaller than the scale of the boundaries of the flow, the Richardson cascade effectively wipes out all information about the large scale geometry, and the velocity increments become statistically homogeneous and isotropic. This is what is referred to as fully developed turbulence. It implies that the structure functions only depend on the length scale l:

$$S_p(\mathbf{x}, \mathbf{l}, t) = S_p(l) \tag{37}$$

That is, the statistical behaviour of velocity increments between two points in space, expressed through the structure functions, only depends on the distance, l, between the two points. Translating the points in space or rotating the vector connecting them, does not change the structure functions.
The first order structure function, $S_1(l)$, is interpreted as the characteristic velocity difference in an eddy of size l. This gives a connection to the Richardson picture.

The second assumption listed above, states that there is a range of length scales, called the inertial range, where dissipation is negligible and the statistical properties of the velocity increments are universally determined by the length scale itself and the average dissipation rate. Because the fluid is in forced steady state, the average dissipation rate is equal to the forcing. The dimensions of the structure function and the average energy dissipation rate are

$$\big[S_p(l)\big] = \frac{length^p}{time^p}$$

$$\big[\bar{\epsilon}\big] = \frac{length^2}{time^3}$$

By dimensional analysis the only possible relation is then

$$S_p(l) = C_p\big(\bar{\epsilon} l\big)^{p/3} \tag{38}$$

Where C_p is a universal constant. These power laws are the celebrated K41 scaling relations. They predict that there is an inertial range, where the flow is statistically self similar. A connection can be made with the Richardson cascade, if one interprets the first order structure function, $S_1(l)$, as the characteristic velocity difference in an eddy of size l. The characteristic velocity difference will scale as $l^{1/3}$, and the flow will look similar on all length scales in the inertial range.

The lower bound of the inertial range, η, is called the dissipation or Kolmogorov scale. It is the length scale at which dissipation becomes important, assuming that the energy spectrum scales as (39). That is

$$\nu v_i \partial_{jj} v_i \sim \nu S_2(\eta)/\eta^2 \sim \nu \eta^{-4/3} \epsilon^{2/3} \sim \epsilon$$

so that

$$\eta \sim \left(\frac{\epsilon}{\nu^3}\right)^{-1/4}$$

An analogous argument, as the one made about the structure functions, can be made about the energy spectrum of the fluid, defined in equation (28). The energy spectrum has the dimensions

$$\big[E(k)\big] = \frac{length^3}{time^2}$$

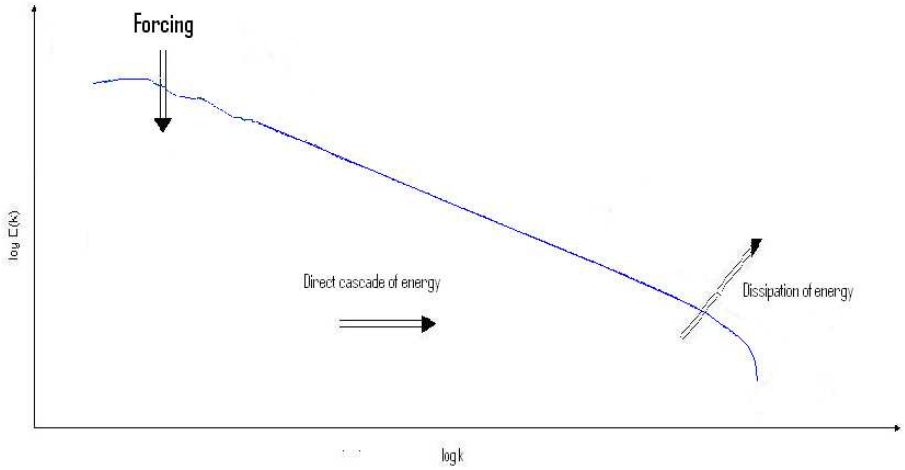

Figure 8: The figure shows an illustration of a steady state in 3D turbulence, where energy is cascaded to and dissipated at small length scales

The K41 scaling assumptions then leads to the scaling relation

$$E(k) \propto \bar{\epsilon}^{2/3} k^{-5/3} \tag{39}$$

This scaling relation can also be derived from an exact relation existing between the second order structure function and the energy spectrum for fully developed turbulence(See [*Ditlevsen*, 2004, p. 16]).

Figure (8) shows an illustration of the forced steady state in 3D turbulence. Energy is put in to the flow on large scales by forcing, and is then cascaded through the inertial range, in which energy dissipation is negligible. In this range, the energy flux must be constant if energy is not to build up. Finally, the energy is dissipated at the Kolmogorov scale.

2.2.4 Scaling exponents

K41 theory has been shown hold approximately in numerous experiments. There are, however corrections to the scaling exponents of the structure functions, that are not yet fully understood. Experiments show that there is and inertial range, where the structure functions scale as a power law

$$S_p(l)^{\zeta(p)}$$

but the scaling exponents, $\zeta(p)$, show corrections to the K41 prediction, $p/3$. Figure 9 shows the scaling exponents $\zeta(p)$ measured in a wind tunnel experiment [*F. Anselmet and Antonia*, 1984]. The straight line represent the K41 prediction. One notices that the K41 prediction and the scaling exponents agree very well for the third order structure function. The K41 scaling relations are solely derived by dimensional analysis and have no connection to the NSE's. There is, however, an exact relation for the third order longitudinal structure function, called the 4/5-law:

$$S_3^{\parallel}(l) = \left\langle \delta v_{\parallel}(\mathbf{x}, \mathbf{l}, t) \right\rangle = -\frac{4}{5}\bar{\epsilon} l \tag{40}$$

where

$$\delta v_{\parallel}(\mathbf{x}, \mathbf{l}, t) = \left[\mathbf{v}(\mathbf{x}+\mathbf{l}, t) - \mathbf{v}(\mathbf{x}, t)\right] \cdot \frac{\mathbf{l}}{l}$$

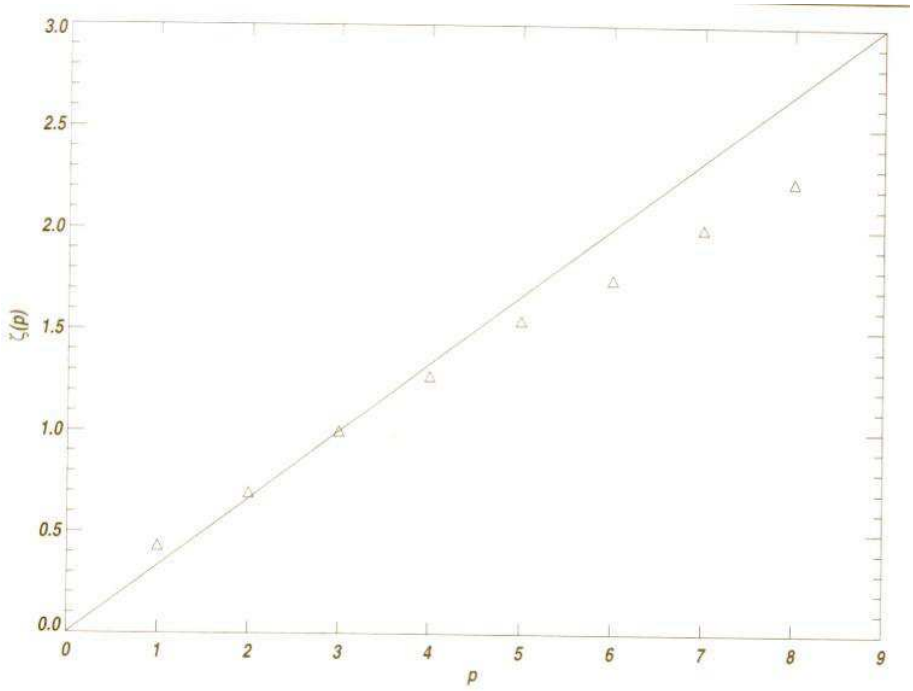

Figure 9: The figure shows scaling exponents seen in a wind tunnel experiment [*F. Anselmet and Antonia*, 1984]

is the longitudinal component of the velocity increment. The relation can be derived from the NSE's, the statistical homogeneity and isotropy of the flow, and the fact that the energy flux must be constant in the inertial range(see [*Ditlevsen*, 2004, p. 20]). It is one of the only exact relations known for turbulence.

The corrections to the scaling exponents are referred to as intermittency corrections, because they are believed to be caused by the intermittency of the flow(see see [*Frisch*, 1995, p. 120]).

2.3 Turbulence in 2D

This section will discuss Kraichnans double cascade scenario for turbulence in a 2D fluid. Turbulence in a 2D fluid is very different from turbulence in a 3D fluid. As described in section 2.1.2, the flow of a 2D fluid has an extra conserved integral in the unforced, inviscid limit, called the enstrophy. This quantity is a strictly positive quantity like energy, and in steady state turbulence for a 2D fluid, both the energy and enstrophy input must be balanced by dissipation.

It can be shown that the ratio of energy and enstrophy dissipation at wave vectors with length k is k^{-2} and that this prohibits a forward cascade of energy(see [*Ditlevsen*, 2004, p. 34]). This led R. H. Kraichnan to propose a different scenario for turbulence in a 2D fluid. Instead of a direct cascade of energy towards smaller scales, he argued that the energy would be cascaded to larger scales in an inverse cascade, and eventually be dissipated by friction at the boundaries of the system. Enstrophy on the other hand would be cascaded towards smaller scales in a direct cascade. This is referred to as the Kraichnan double cascade.

An analogous universality argument, as the on made about the energy spectrum, can be made about the enstrophy spectrum in the enstrophy cascade. The dimensions of the

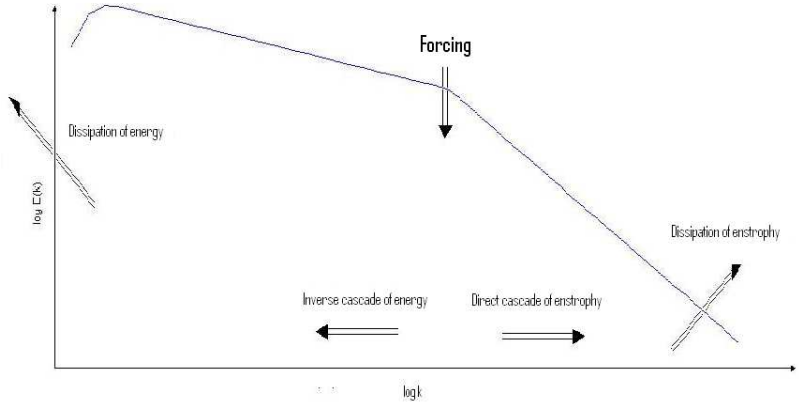

Figure 10: The figure shows an illustration of the Kraichnan double cascade idea of 2D turbulence. A steady state where energy is cascaded to and dissipated at large length scales, and enstrophy is cascaded to and dissipated at small length scales

enstrophy spectrum and the average enstrophy dissipation per mass, $\bar{z}$, are

$$\left[Z(k)\right] = \frac{length}{time^2}$$

$$\left[\bar{z}\right] = \frac{1}{time^3}$$

By dimensional analysis the only possible relation is then

$$Z(k) \propto \bar{z}^{2/3} k^{-1} \tag{41}$$

This means that the energy spectrum scales as

$$E(k) \propto \bar{z}^{2/3} k^{-3} \tag{42}$$

in the direct cascade of enstrophy.

An illustration of the proposed scenario for a 2D fluid is shown in figure 10. Energy and enstrophy is put in to the fluid at intermediate wave numbers. The energy is cascaded to smaller wave numbers where it is dissipated and enstrophy to higher wave numbers where it is dissipated. There is an inertial range for energy where the energy flux is constant and an inertial range for enstrophy where the enstrophy flux is constant.

2.4 Stochastic variables and processes

The models investigated in this thesis are stochastic processes. Therefore, this section gives a short review of stochastic processes, stochastic variables and basic probabilistic concepts. The section does not describe any physics and may be skipped by the reader familiar with the concepts.

2.4.1 Stochastic variables

Stochastic variables are used to describe random events. That is, events where each outcome has an associated probability. Examples might be the flipping of a coin or the the time between counts in a Geiger apparatus. More precisely, a stochastic variable, $\hat{X}$, maps the set of possible outcomes of a random event into the real numbers or a subset of these. That is, it associates with every outcome of a probabilistic event, a real number. If S denotes the space of possible outcomes, and Ω, a subset of the real numbers, then

$$\hat{X} : S \to \Omega$$

Ω is called the configuration space of the stochastic variable. In the coin example, there are two possible outcomes: Heads or tail. The random variable might map heads in to -1 and tails in to 1.
In the second example of a Geiger apparatus, the set of outcomes are simply all the possible durations of time between two counts. The stochastic variable might map this set of outcomes into a time measured in second, nanoseconds or any other time unit.

There is an obvious difference between the two examples. In the first, configuration space is discrete(i.e the stochastic variable can only take on a discrete set of values), $\Omega = \{1, -1\}$, while in the second, configuration space is continuous, $\Omega = \mathbb{R}^+$. One refers to a stochastic variable as either discrete or continuous.
In order to describe the probabilities of each event, the stochastic variable has an associated probability function or probability density. A discrete stochastic variable, $\hat{X}$, has an associated probability function $p(x)$, that gives the probability that $\hat{X} = x$:

$$\text{Prob}(\hat{X} = x) = p(x) \tag{43}$$

A continuous random variable, $\hat{X}$, has an associated probability density, $p(x)$, such that the probability of $\hat{X}$ lying in the infinitesimal interval $[x, x + dx]$ is $p(x)dx$:

$$\text{Prob}(x \leq \hat{X} \leq x + dx) = p(x)dx \tag{44}$$

The sensible requirement that something must happen, is assured by the normalisation of the probability function in the discrete case and the probability density in the continuous case:

$$\sum_{\Omega} p(x) = 1 \tag{45}$$

$$\int_{\Omega} p(x)dx = 1 \tag{46}$$

In the following, only continuous stochastic variables will be considered.

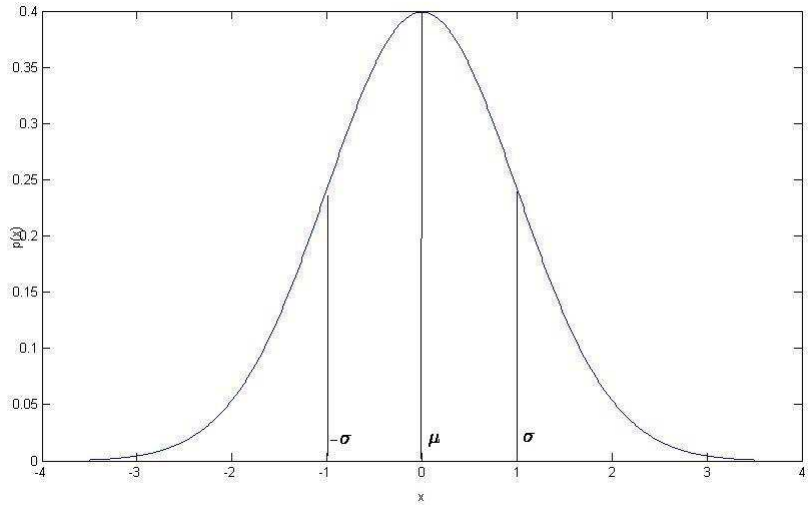

Figure 11: The figure shows a Gauss distribution with mean 0 and variance 1

One can find the expectation value, denoted $\langle ... \rangle$, with respect to a probability density. The expectation value of a function f is defined as

$$\langle f(x) \rangle = \int_{\Omega} f(x)p(x)dx \tag{47}$$

The expectation value of different powers of the stochastic variable, called the moments of the probability density, are of special interest, because they characterise the probability density. The m'th order moment is defined as

$$< x^m >= \int_{\Omega} m^m p(x)dx \tag{48}$$

The first order moment, $< x >$, gives the average value of the stochastic variable. Combining the first and second order moments, one can construct the variance, defined as:

$$\sigma^2 = \langle (x- < x >)^2 \rangle = \int_{\Omega} (x- < x >)^2 p(x)dx =< x^2 > - < x >^2 \tag{49}$$

The square root of the variance, σ, is called the mean square displacement, and measures the spread of the probability density. Many other combinations of moments can be used to describe the characteristics of a probability density.
Figure 11 shows a gaussian probability density, with the first order moment and mean square displacement marked.

2.4.2 Stochastic vectors

Stochastic vectors, also called multivariate stochastic variables, are a generalisation of stochastic variables. Instead of mapping the probabilistic event into a scalar number, they map it into a vector. If we look at an N-dimensional stochastic vector, there is an associated joint probability density, $p(\mathbf{x}) = p(x_1, x_2, ..., x_N)$, which is a function of N variables. The probability that the stochastic vector, $\hat{\mathbf{X}}$, will take on a value within an infinitesimal hypercube around $\mathbf{x}$ is:

$$\text{Prob}(\mathbf{x} \leq \hat{\mathbf{X}} \leq \mathbf{x} + d\mathbf{x}) = p(\mathbf{x})d\mathbf{x} \tag{50}$$

The generalisation of the expectation value (47) is straight forward:

$$\langle f(\mathbf{x}) \rangle = \int_{\Omega} f(\mathbf{x})p(\mathbf{x})d\mathbf{x} \tag{51}$$

Given a stochastic vector, an obvious question might be: What is the interdependence between the different variables. Two variables, x_i and x_j are said to be independent if we can separate the probability density

$$p(x_i, x_j) = p_i(x_i)p_j(x_j) \tag{52}$$

If two variables are not independent, their degree of dependency can be expressed through a statistical measure, called the correlation. If we once again look at an N-dimensional stochastic vector, the correlation matrix, ρ, is defines by it's entries as:

$$\rho_{ij} = \frac{\langle (x_i - < x_i >)(x_j - < x_j >) \rangle}{\sqrt{\sigma_i \sigma_j}} \tag{53}$$

The correlation matrix is symmetric and has a unit diagonal. The rest of the entries can be shown to lie between -1 and 1, by using the Cauchy-Schwarz inequality(See appendix). The off-diagonal entry ρ_{ij} measures the correlation between the two elements x_i and x_j in the stochastic vector. The elements are said to be negatively correlated if $\rho_{ij} < 1$, positively correlated if $\rho_{ij} > 1$ and uncorrelated if $\rho_{ij} = 0$. If x_i and x_j are independent, in the sense of equation (52), they are uncorrelated. The converse is not nessesarily true.

2.4.3 Stochastic processes

Some systems evolve according to probabilistic rules, or the dynamics are so complicated that a probabilistic description is preferable. Such a system can be described by a stochastic process.
In the following we consider an N-dimensional stochastic vector process, $\hat{\mathbf{X}}(t) = \left(\hat{X_1}(t), \hat{X_2}(t), ..., \hat{X_N}(t)\right)$, that is continuous in time.

Such a stochastic process is fully described if we know the joint probability density $p(\mathbf{x_1}, t_1; \mathbf{x_2}, t_2; ...; \mathbf{x_M}, t_M)$, for all possible sets of times $[t_1, t_2, ..., t_M]$. $p(\mathbf{x_1}, t_1; \mathbf{x_2}, t_2; ...; \mathbf{x_M}, t_M)d\mathbf{x_1}d\mathbf{x_2}...d\mathbf{x_M}$ is interpreted as the probability that the random variable at time t_1, lies in the N-dimensional hypercube $[\mathbf{x_1}, \mathbf{x_1} + d\mathbf{x_1}]$, at time t_2, in the hypercube $[\mathbf{x_2}, \mathbf{x_2} + d\mathbf{x_2}]$ and so forward. That is

$$\text{Prob}\Big(\mathbf{x_1} \leq \hat{\mathbf{X}}(t_1) \leq \mathbf{x_1} + d\mathbf{x_1},\, \mathbf{x_2} \leq \hat{\mathbf{X}}(t_2) \leq \mathbf{x_2} + d\mathbf{x_2}\,, ...,\, \mathbf{x_M} \leq \hat{\mathbf{X}}(t_M) \leq \mathbf{x_M} + d\mathbf{x_M}\Big) \tag{54}$$

$$= p(\mathbf{x_1}, t_1; \mathbf{x_2}, t_2; ...; \mathbf{x_M}, t_M)d\mathbf{x_1}d\mathbf{x_2}...d\mathbf{x_M} \tag{55}$$

A natural question when looking at a stochastic vector process is: How are the different variables correlated at different times. This can be expressed trough the autocovariance matrix:

$$\Gamma_{ij}(t_1, t_2) = \Big\langle \Big(x_i(t_1) - \langle x_i(t_1) \rangle\Big)\Big(x_j(t_2) - \langle x_j(t_2) \rangle\Big) \Big\rangle \tag{56}$$

The autocovariance matrix is closely related to the autocorrelation matrix, trough the relation

$$\rho_{ij}(t_1, t_2) = \frac{\Gamma_{ij}(t_1, t_2)}{\sqrt{\sigma_i(t_1)\sigma_j(t_2)}} \tag{57}$$

Where $\sigma_i(t)$ is the variance of the i'th variable at time t. When $t_1 = t_2 = t$, the autocorrelation matrix is just the correlation matrix given in equation 53, and gives the correlation between the different variables at time t. Otherwise it gives a measure of the correlation between the stochastic variables at different times t_1 and t_2. The case $i = j$ is of special interest: The diagonal element $\rho_{ii}(t_1, t_2)$ is called the autocorrelation function of the i'th variable, and gives the correlation of the variables with itself, at different points in time.

Certain stochastic process have the property of being stationary. A process is stationary to the N'th order

$$p(x_1, t_1; x_2, t_2; ...; x_N, t_N) = p(x_1, t_1{+}\tau; x_2, t_2{+}\tau; ...; x_n, t_n{+}\tau) \quad \text{, for all } \tau \text{ and } n = \{1, 2, 3, ...N\} \tag{58}$$

That is, the joint probability density of any sets of $n = \{1, 2, 3, ...N\}$ variables, looks the same, if we translate it in time.
A less strict requirement, is that a process is weakly stationary. Weak stationarity requires that the first order moment is time independent, and that the autocovariance matrix only depends on the time difference:

$$< x_i(t) >=< x_i > \quad \text{for all } i$$

$$\Gamma_{ij}(t_1, t_2) = \Gamma_{ij}(t_2 - t_1) \quad \text{for all } i, j$$

The last requirement, implies that the variance is time independent.
A process that is second order stationary and has a well defined mean and variance, is also weakly stationary.
A stochastic process, may not be weakly stationary, at first, but approach weak stationarity in time. In this case

$$< x_i(t) >=< x_i > \quad \text{for all } i \text{ and } t > T$$

$$\Gamma_{ij}(t_1, t_2) = \Gamma_{ij}(t_2 - t_1) \quad \text{for } t > T$$

Where T is the time it takes to reach weak stationarity.

2.4.4 The Poisson process

The Poisson process is central to the cascade models that will be introduced in section 3, and serves as an example of a stochastic process. The process is widely used, when modelling events that are randomly and homogeneously distributed in time.
The Poisson process, $N(t)$, counts the number of occurrences of some event in the time interval $[0, t]$. It is characterised by the rate parameter λ; the rate with which events occur. The probability of l occurrences in a time interval Δt is:

$$P\big[N(t + \Delta t) - N(t) = l\big] = \frac{e^{-\lambda \Delta t}(\lambda \Delta t)^l}{l!} \tag{59}$$

This is the probability distribution of the increment in $N(t)$, and it only depends on the rate parameter and the length of the time interval. The probability distribution for $N(t)$ is given by the above expression, with $t = 0$ and $N(0) = 0$ The Poisson is not

stationary, since the above distribution has both mean and variance that grows linearly in time as $\lambda\Delta t$. It is continuous in time, but has discrete configuration space.

A variation of the Poisson process that will be relevant for the cascade models, is the non-homogeneous Poisson process. Instead of having a constant rate parameter, the rate is a function of time:

$$\lambda = \lambda(t)$$

The probability of l events in a time interval Δt is:

$$P\big[N(t+\Delta t) - N(t) = l\big] = \frac{e^{-h}h^l}{l!} \tag{60}$$

where

$$h = \int_t^{t+\Delta t} ds\ \lambda(s) \tag{61}$$

For small Δt, the probability function can be Taylor expanded to

$$P\big[N(t+\Delta t) - N(t) = 1\big] = \Delta t\lambda(t) + o(\Delta t) \tag{62}$$

and

$$P\big[\Delta N_n^{ET}(t,\Delta t) > 1\big] = o(\Delta t) \tag{63}$$

Here, $o(\Delta t)$ represents higher order terms in Δt.
In the non-homogeneous Poisson process events are no longer homogeneously distributed in time.

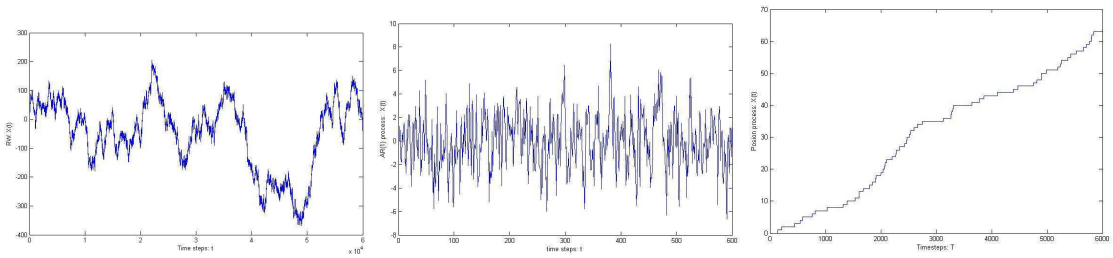

Figure 12: Realisation of symmetric random walk(left), an AR(1) process(middle) and a Poison process(right)

2.5 Time series analysis

The two cascade models that are investigated in the thesis(to be introduced in section 3) are stochastic processes. The models have been simulated on a computer, as will be described in section 4. Such simulations produce single realizations of the stochastic processes, referred to as time series. This section is dedicated to introducing tools used in the analysis of time series.

A time series is a realization of a stochastic process. Figure 12 shows 3 examples of time series: The figure on the left shows a realization of a symmetric random walk, the middle figure, a first order auto-regressive model(AR(1)) and the figure on the right, a Poisson process. The 3 time series clearly behave differently. The first time series seem to have a growing variance, but a constant mean. The second time series seem to have both a constant mean and variance. While the third series looks to have a mean and variance that are both growing in time.

In the three examples we know the processes of which the time series are realizations. In general, the aim of analysing time series is to gain knowledge of the stochastic processes underlying the data. One might be investigating a stochastic differential or difference equation that can not be solved analytically, by simulating the process on a computer. This is the type of problem investigated in this thesis. Alternatively, one might be looking at real world data, and treat the data as though it reflects an unknown underlying stochastic process.

In any event, we imagine that we have data points at a number of times $t_1, t_2, t_3, .., t_M$, and that these data point are a realization of a N-dimensional stochastic vector process, $\hat{\mathbf{X}}(t) = \big(\hat{X}_1(t), \hat{X}_2(t), ..., \hat{X_N}(t)\big)$, with some unknown probability density $p(\mathbf{x_1}, t_1; \mathbf{x_2}, t_2; ...; \mathbf{x_M}, t_M)$. For convenience, we assume that the data points are equally spaced in time, $t_j = j\Delta t$, and we denote the stochastic variable at time t_j by $\hat{\mathbf{X}}(j)$.
In the following we will also assume that we are looking at realizations of a weakly stationary process. As described in the previous section, this means that the mean of the process is time independent and that the autocovariance only depends on the time difference:

$$\big\langle x_i(j) \big\rangle = \int_\Omega d\mathbf{x} \;\; p(\mathbf{x}, t_j) x_i = \mu_i \tag{64}$$

$$\Gamma_{ij}(l,k) = \Big\langle \Big(x_i(l) - \big\langle x_i(l) \big\rangle \Big) \Big(x_j(k) - \big\langle x_j(k) \big\rangle \Big) \Big\rangle = \Gamma_{ij}(l-k) \tag{65}$$

Our aim of analysing a time series will be to estimate the mean and variance of the process. For this we need what is called estimators.

As an estimator of the mean of the i'th component of the stochastic process we use

$$m_i = \frac{1}{M}\sum_{j=1}^{M} \hat{X}_i(j) \tag{66}$$

m_i is the sum of the stochastic process at all the sample times, divided by the number of sample times, and is itself a stochastic variable, with a probability distribution. For a single time series, m_i is just the sample average. The expectation value of m_i coincides with the mean of the process.

$$\langle m_i \rangle = \Big\langle \frac{1}{M}\sum_{j=1}^{M} x_i(j) \Big\rangle = \frac{1}{M}\sum_{i=1}^{M} \langle x_i(j) \rangle = \mu_i \tag{67}$$

One says that the estimator is unbiased. This does not, however, ensure that m_i is a good estimator. If the variance of m_i is huge, we will have a large error on the estimate.

We now calculate the variance of m_i. In order to ease the notation, we drop the subscript i, so that $m_i = m$, $\mu_i = \mu$, $\Gamma_{ii}(l-j) = \Gamma(l-j)$ and $\rho_{ii}(k-j) = \rho(k-j)$.

$$\begin{aligned}
\sigma_m^2 =& \langle (m-\mu)^2 \rangle =< m^2 > +\mu^2 - 2\mu < m > \\
=& < m^2 > -\mu^2 = \frac{1}{M^2}\sum_{i=j}^{M}\sum_{l=1}^{M} \langle x(j)x(l) \rangle - \mu^2 \\
=& \frac{1}{M^2}\sum_{j=1}^{M}\sum_{l=1}^{M} \big(\Gamma(l-j) + \mu^2\big) - \mu^2 = \frac{\sigma^2}{M} + \frac{2}{M^2}\sum_{j=1}^{M-1}(M-j)\rho(j) \\
=& \frac{\sigma^2}{M}\Big[1 + \frac{2}{M}\sum_{j=1}^{M-1}(M-j)\rho(j)\Big]
\end{aligned} \tag{68}$$

Where it has been used that the process is weakly stationary, and σ^2 is the time independent variance of $\hat{X}_i$.
If the correlation time is finite(i.e. $\rho(j) \to 0$ when $j \to \infty$), the above expression for the variance will go to zero as M goes to infinity. This is what we want in our estimator: That when the number data points grows, the estimate(an outcome of the estimator) becomes more precise.
If the stochastic process has no correlation in time, we get the well known result that the error in the estimate falls of as $\frac{\sigma}{\sqrt{M}}$

We now look at an estimator for the variance. A first guess might be the sample average

$$\tilde{\sigma}_i = \frac{1}{M}\sum_{i=1}^{M}(\hat{X}_i(j) - m_i)^2 \tag{69}$$

However, this estimator turns out to be biased. Taking the expectation value, and again dropping the subscript i, we get:

$$\left\langle \tilde{\sigma}^2 \right\rangle = \frac{1}{M}\sum_{j=1}^{M}\left\langle (x(j)-m)^2 \right\rangle = \frac{1}{M}\sum_{j=1}^{M}\left\langle \big((x(j)-\mu)-(m-\mu)\big)^2 \right\rangle \tag{70}$$

$$= \sigma^2 + \sigma_m^2 - 2\Big\langle (m-\mu)\frac{1}{M}\sum_{j=1}^{M}\big(x(j)-\mu\big)\Big\rangle = \sigma^2 - \sigma_m^2$$

The estimator is biased, because it involves the estimator of the mean. It will underestimate the variance of the process, if the correlation function $\rho(j)$ is positive. To get an unbiased estimator, we insert the expression for the variance of the mean given in equation (68) and isolate the variance of the process to get:

$$\sigma^2 = \frac{N}{N-1-\kappa}\left\langle \tilde{\sigma}^2 \right\rangle \tag{71}$$

Where we have introduced

$$\kappa = \frac{2}{N}\sum_{j=1}^{N}(N-j))\rho(j)$$

This is a correction due to correlations in time.
From the expression (71), we see that the following estimator for the variance is unbiased

$$s = \frac{1}{N-1-\kappa}\sum_{i=1}^{N}(\hat{X}_i - m)^2 \tag{72}$$

If one has an analytical expression for the correlation function $\rho(j)$, an unbiased estimate for variance can be found by (72). Then the error on the estimate of the mean, σ_m, can in turn be estimated from (68).

Unfortunately, in the models investigated in the thesis, we do not have an analytical expression for the correlation function. Therefore we do not know the correction κ, and do not know the bias of the estimator (69).

Lacking a better approach, the biased estimator

$$\rho_{ij}(l) = \frac{1}{M-j}\sum_{k=1}^{M-l}(\hat{X}_i(l) - m_i)(\hat{X}_j(1) - m_j) \tag{73}$$

has been used to estimate the autocorrelation matrix, from the simulations of the models. When the number of sampling points, M, is large compared to the correlation time, the bias on this estimate will be very little. The correction will be of the order T_{corr}/M, where T_{corr} is the correlation time. From the estimated autocorrelation matrix, the error on the estimate of the mean has then been estimated by equation (68).

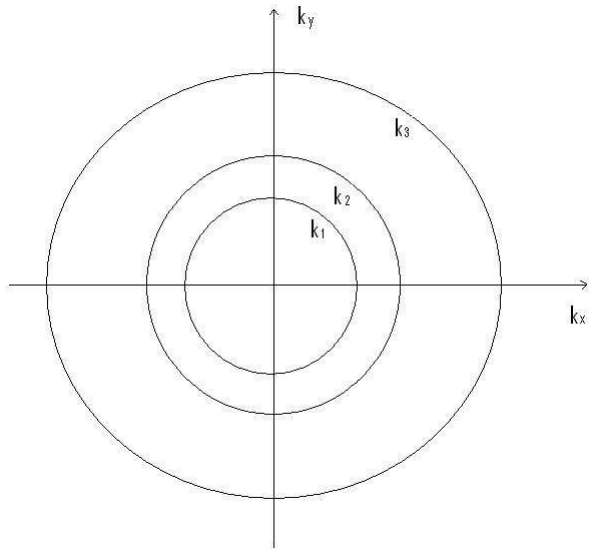

Figure 13: The figure shows the 3 first shells in a 2 dimensional k-space. The radius of the shells are growing exponentially with shell number

3 Two stochastic cascade models

The aim of this section is to introduce two stochastic cascade models:

- A model of two dimensional turbulence, that conserves energy- and enstrophy-like quantities, in the inviscid, unforced limit.
- A model of three dimensional turbulence, that conserves energy- and helicity-like quantities, in the inviscid, unforced limit.

The first part of the section, presents the common structure of the 2D and 3D models. In the following two parts, the local triad interactions, specific to the two- and three-dimensional case are described.

3.1 Common structure

The models are constructed to have a flavour of the differential equations for the spectral energy density in (24), that is derived from the NSE's.
However, the number of Fourier modes is severely truncated, by partitioning k-space into a number of shells. These shells have radius that are equidistant on a logarithmic scale:

$$k_n = \lambda^n \tag{74}$$

where $\lambda > 1$, and $n = 1, ..., N$.
Figure 13 shows 3 such shells in a two dimensional k-space.

For each shell, n, the models have one degree of freedom; the shell energy $E_n(t)$. The shell energies can be viewed as the integral of the spectral energy density (22) over $\mathbf{k}$-values between adjacent shells.

$$E_n(t) = \int_{\|\mathbf{k}\| \geq k_n}^{\|\mathbf{k}\| < k_{n+1}} E(\mathbf{k}, t) d\mathbf{k} \tag{75}$$

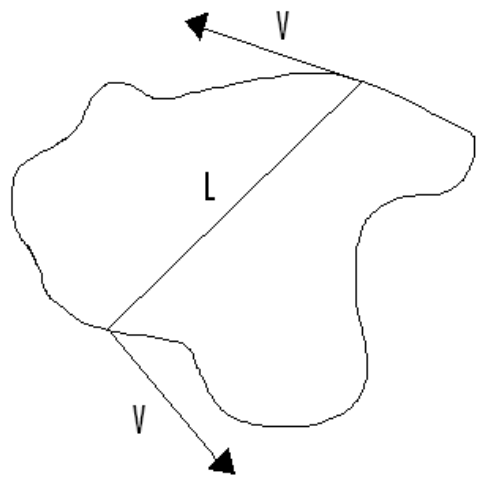

Figure 14: The figure shows an eddy of characteristic size L and with a characteristic velocity V. The typical deformation time will be L/V. This is refered to as the eddy turnover time

The number of degrees of freedom in the models, N, will be related to a cut-off wavenumber K_{cut}, as $N \propto \log(K_{cut})$. By comparison, the number of degrees of freedom in the NSE's for a d-dimensional fluid, scales as K_{cut}^d.

3.2 Eddy-turnovers

We shall think of the shell energy E_n, as the energy present in eddies of size $l_n = 1/k_n$. The energy can be redistributed locally among the shells in events that we will refer to as eddy turnovers.
An eddy turnover takes place on a particular shell, and the redistribution of energy only involves a local triad of shells.
The actual way in which energy is redistributed among the shells in an eddy turnover is specific to the 2D and 3D models, and will be introduced in section 3.3 and 3.4.

First, we look at the number of eddy turnovers on a particular shell, n, which we denote N_n^{ET}. The central idea of the models, is that this is a non-homogeneous Poisson process.
A non-homogeneous Poisson process is characterized by the average time between events, through the rate parameter(see section 60). We will denote the average time between two eddy turnovers on the n'th shell by τ_n, and refer to it as the characteristic eddy-turnover time.

Intuitively, the average time between eddy turnovers on the n'th shell, must be the time it typically takes an eddy of size l_n to deform. Since a typical velocity at the length scale l_n, is $\sqrt{E_n(t)}$, we construct the characteristic eddy-turnover time to be:

$$\tau_n(t) = \frac{l_n}{\sqrt{E_n(t)}} = \frac{1}{k_n\sqrt{E_n(t)}} \tag{76}$$

A drawing of the idea, is shown in figure 14. Notice that the eddy-turnover time is dynamical, as it depends on the energy.

Since the rate parameter of the non-homogeneous Poisson process is τ_n^{-1}, the probability of l eddy-turnovers in the time interval T is

$$P\big[N_n^{ET}(t+T) - N_n^{ET}(t) = l\big] = \frac{e^{-h}h^l}{l!} \tag{77}$$

where

$$h = \int_t^{t+T} ds \frac{1}{\tau_n(s)} \tag{78}$$

The Poisson process is non-homogeneous because the eddy turnover time, τ_n, depends on $E_n(t)$ through equation (76). However, the vector of shell energies, $\mathbf{E}(t) = \big(E_1(t), E_2(t), E_3(t), ..., E_N(t)\big)$, will be a stochastic process, so we do not have an analytic expresion for the the eddy turnover time. Therefore, performing the integral (78) is not possible.
We can, however, describe the probability of an eddy turnover if we look at a small time interval. We define a stochastic variable that gives the increment in the number of eddy turnovers:

$$\Delta N_n^{ET}(t, \Delta t) = N_n^{ET}(t + \Delta t) - N_n^{ET}(t) \tag{79}$$

In a small time interval Δt, we have

$$P\big[\Delta N_n^{ET}(t, \Delta t) = 1\big] = \frac{\Delta t}{\tau_n(t)} + o(\Delta t) \tag{80}$$

and

$$P\big[\Delta N_n^{ET}(t, \Delta t) > 1\big] = o(\Delta t) \tag{81}$$

Here, $o(\Delta t)$ represents higher order terms in Δt. We are assuming that the eddy-turnover time does not change in the small time interval Δt. The argument is that the probability of two or more eddy turnovers is higher order in Δt.

3.3 2D model

This section describes the local eddy turnover rules for the 2D model.
In case of an eddy turnover on the n'th shell, the energy is redistributed within the triad $(n-1, n, n+1)$ in one of the 3 ways shown in figure 15.
We label the 3 different types of eddy turnovers shown in the figure as a loss event(L), a gain event(G) and no event(N).
In loss or gain events, the energy is redistributed according to the following rules:

$$\begin{aligned} E_n &\longrightarrow E_n \mp q\Delta_n \\ E_{n+1} &\longrightarrow E_{n+1} \pm q\frac{\epsilon - 1}{\epsilon}\Delta_n \\ E_{n-1} &\longrightarrow E_{n-1} \pm \frac{q}{\epsilon}\Delta_n \end{aligned} \tag{82}$$

Where the first sign refers to a loss event and the second sign to a gain event. In case of no event, the shell energies in the triad remain the same.
The expressions for gain and loss events involve two model parameters, ϵ and q, and a dynamical quantity, Δ_n, that depends on the shell energies. Δ_n is the amount of energy

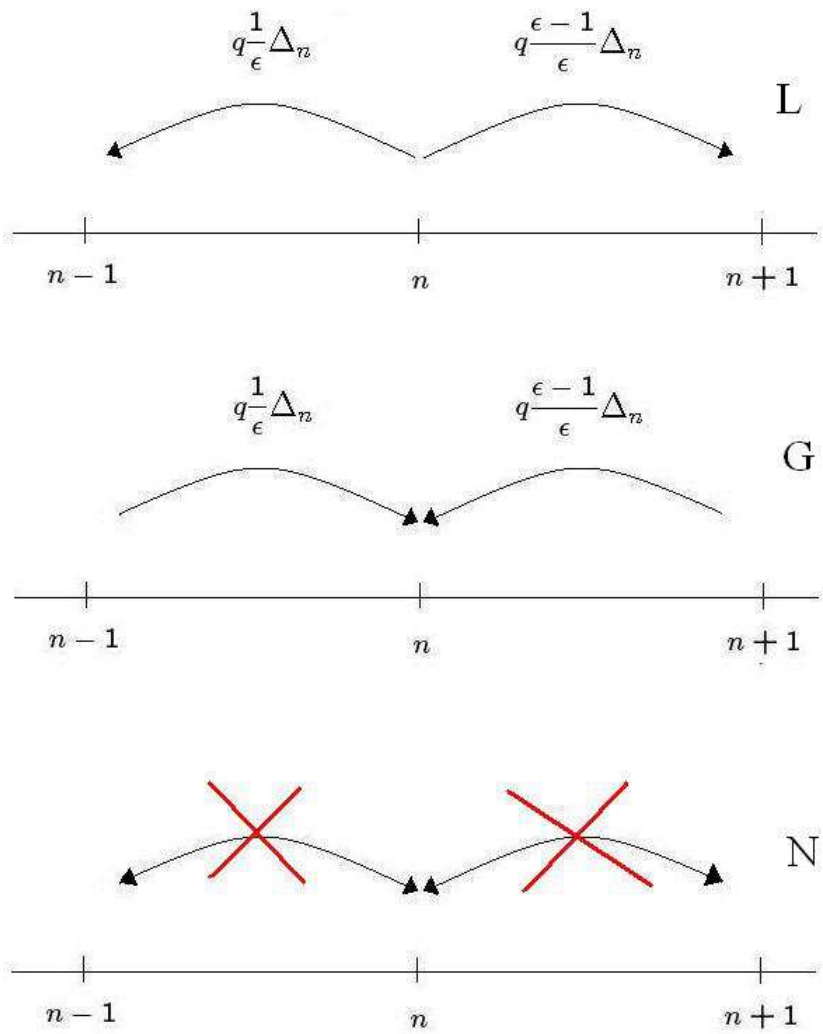

Figure 15: The figure shows the 3 possible outcomes of an eddy at shell n, for the 2D model. A loss event(L), a gain event(G), and no event(N)

that is redistributed in a jumping or a sucking event. We consider two different expressions for it in the thesis:

$$\Delta_n = E_n \tag{83}$$

and

$$\Delta_n = \left(E_{n-1}E_nE_{n+1}\right)^{1/3} \tag{84}$$

The two parameters ϵ and q are restricted to the intervals

$$q \in [0,1]$$

and

$$\epsilon \in [1,2]$$

q determines how big a portion of the quantity Δ_n is involved in the eddy turnover. ϵ determines the redistribution.
If $\epsilon = 2$, all of the quantity $q\Delta_n$ is exchanged between the shell n, where the eddy turnover takes place, and the shell of lower wave number$(n-1)$.
If $\epsilon = 1$, equal amounts of the quantity $q\Delta_n$ is being exchanged with the shell of lower wave number$(n+1)$ and the shell of higher wave number$(n+1)$. The transformation $\epsilon \to -\epsilon$ would exchange the roles of jumping and sucking events. In section 3.5 it will be shown that ϵ also determines the form of an enstrophy-like inviscid invariant.

The 3 types of events(L, G and N) are constructed to happen with certain probabilities that depend on the shell energies.
If $E_n > q\Delta_n$, $E_{n-1} > \frac{q}{\epsilon}\Delta_n$ and $E_{n+1} > q\frac{\epsilon-1}{\epsilon}\Delta_n$, these probabilities are:

$$P_n^L(\mathbf{E}) = \begin{cases} \frac{1}{2}\frac{E_n}{\sqrt{E_{n-1}E_{n+1}}} & \text{, for } \frac{E_n}{\sqrt{E_{n-1}E_{n+1}}} < 2 \\ 1 & \text{, for } \frac{E_n}{\sqrt{E_{n-1}E_{n+1}}} \geq 2 \end{cases} \tag{85}$$

$$P_n^G(\mathbf{E}) = \begin{cases} 1 - \frac{1}{2}\frac{E_n}{\sqrt{E_{n-1}E_{n+1}}} & \text{, for } \frac{E_n}{\sqrt{E_{n-1}E_{n+1}}} < 2 \\ 0 & \text{, for } \frac{E_n}{\sqrt{E_{n-1}E_{n+1}}} 2 \end{cases} \tag{86}$$

$$P_n^N(\mathbf{E}) = 0 \tag{87}$$

Otherwise the probabilities are

$$P_n^L(\mathbf{E}) = 0 \tag{88}$$

$$P_n^G(\mathbf{E}) = 0 \tag{89}$$

$$P_n^N(\mathbf{E}) = 1 \tag{90}$$

This is a somewhat cumbersome construction, but it is necessary to ensure that the energies can not become negative. Notice that if one of the inequalities $E_n < q\Delta_n$, $E_n - 1 < \frac{q}{\epsilon}\Delta_n$ or $E_n + 1 < q\frac{\epsilon-1}{\epsilon}\Delta_n$ is fulfilled, either a loss or gain event will result in a negative shell energy for one of the triad of shells.
The probabilities of the 3 outcomes are conditional on the values of the shell energies, and have been constructed such that $P_n^J = P_n^S$ for all scaling relations $E_n \propto k_n^\gamma$.

In order to formulate the dynamics of the model more compactly, a new stochastic variable, X_n, is introduced. The variable is defined to have outcomes 0, 1 and -1 with the probabilities:

$$X_n(t,\Delta t) = \begin{cases} 0 & \text{with probability } \left[1 - \frac{\Delta t}{\tau_n(t)}\left(P_n^L(\mathbf{E}) + P_n^G(\mathbf{E})\right)\right] \\ 1 & \text{with probability } \frac{\Delta t}{\tau_n(t)} P_n^L(\mathbf{E}) \\ -1 & \text{with probability } \frac{\Delta t}{\tau_n(t)} P_n^G(\mathbf{E}) \end{cases} \tag{91}$$

The probability function of X_n depends on the shell energies. In the limit $\Delta t \to 0$, the outcomes of X_n correspond to the following events on the n'th shell: A loss event($X_n = 1$), a gain event($X_n = -1$), and no event($X_n = 0$).

This is because, in the limit $\Delta t \to 0$, the probability of more than one eddy turnover in the time interval Δt goes to zero, so that

$$\Delta N_n^{ET}(t,\Delta t) = \begin{cases} 0 & \text{with probability } \left(1 - \frac{\Delta t}{\tau_n(t)}\right) \\ 1 & \text{with probability } \frac{\Delta t}{\tau_n(t)} \end{cases} \tag{92}$$

This means that the probability of an eddy turnover resulting in a loss event(L) is $\frac{\Delta t}{\tau_n(t)} P_n^L(\mathbf{E})$. That the probability of an eddy turnover resulting in a gain event(G) is $\frac{\Delta t}{\tau_n(t)} P_n^G(\mathbf{E})$. And that the probability of no eddy turnover or a no event(N) in an eddy turnover is $\left[1 - \frac{\Delta t}{\tau_n(t)}\left(P_n^L(\mathbf{E}) + P_n^G(\mathbf{E})\right)\right]$.

With the above notation, the stochastic dynamics can be described by the equation

$$\begin{aligned} E_n(t+\Delta t) - E_n(t) = &- X_n(t,\Delta t)\Delta_n(t) + q\frac{\epsilon - 1}{\epsilon} X_{n-1}(t,\Delta t)\Delta_{n-1}(t) \\ &+ \frac{q}{\epsilon} X_{n+1}(t,\Delta t)\Delta_{n+1}(t) \end{aligned} \tag{93}$$

Where it is assumed that the time increment, Δt, is small enough to justify the assumption, that no more than one eddy turnover can occur.
The l.h.s of equation (93) is the change in the energy on shell n. The first term on the r.h.s is the change in energy that comes about because of an eddy turnover on shell n. The two last terms on the r.h.s describe the change in energy that comes about because of eddy turnovers on the two neighbour shells $n-1$ and $n+1$.
Notice that the triad interactions are local in k-space: Only neighbouring shells interact, as opposed to equation (24) for a real fluid, where wave vectors do not only couple locally. So far the dynamics only include the non linear triad interactions, that govern how energy moves between different length scales. We want the model to incorporate dissipation and forcing as well. Therefore we introduce small and large scale dissipation and external forcing, so that the dynamics become:

$$\begin{aligned} E_n(t+\Delta t) - E_n(t) = &- \left[\nu_1 k_n^2 \Delta t + \nu_2 k_n^{-2} \Delta t\right] E_n(t) - q X_n(t,\Delta t)\Delta_n(t) \\ &+ q\frac{\epsilon - 1}{\epsilon} X_{n-1}(t,\Delta t)\Delta_{n-1}(t) \; + \; \frac{q}{\epsilon} X_{n+1}(t,\Delta t)\Delta_{n+1}(t) \\ &+ \delta_{n,f} F \Delta t \end{aligned} \tag{94}$$

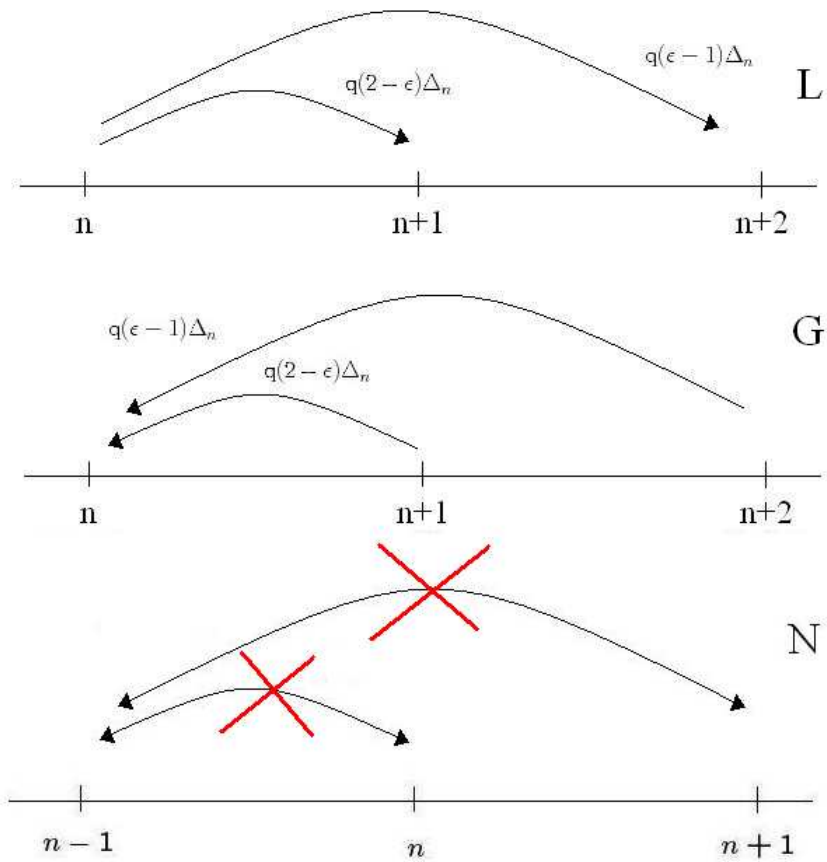

Figure 16: The figure shows 3 possible outcomes in an eddy turnover at shell n for the 3D model. A loss event(L), a Gain event(G) and no event(N)

Here, F is a forcing that takes place solely on shell f, and ν_1 and ν_2 are small and large scale viscosities. The two viscosity terms are linear in the shell energy, as is the case in the differential equation for the spectral energy density (24).

We need some boundary conditions to close the set of equations (94). These are inferred by requiring that eddy turnovers can not take place at the boundary shells. That is

$$X_0(t) = X_1(t) = X_N(t) = X_{N+1}(t) = 0$$

The set of equation (94), the boundary conditions, and an initial condition, $\mathbf{E}(t = 0) = \mathbf{E}_0$, specifies the stochastic process for the 2D model.

3.4 3D model

This section describes the local eddy turnover rules for the 3D model.
In case of an eddy turnover on the n'th shell, the energy is redistributed within the triad $(n, n+1, n+2)$ in one of the 3 ways shown in figure 16.
Again, we label the 3 different types of eddy turnovers shown in the figure as a loss events(L), a gain events(G) and no event(N).
In a loss or gain event the energy is redistributed according to the following rules:

$$E_n \longrightarrow E_n \mp q\Delta_n$$

$$E_{n+1} \longrightarrow E_{n+1} \pm q(2-\epsilon)\Delta_n \tag{95}$$
$$E_{n+2} \longrightarrow E_{n-1} \pm q(\epsilon-1)\Delta_n$$

where the first sign refers to a loss event and the second sign to a gain event. In a no event(N), the triad of shell energies remain unchanged.
Again the expressions involve two model parameters, ϵ and q, and a dynamical quantity, Δ_n, that depends on the shell energies.
The same two expressions for the amount of energy being redistributed, Δ_n, are considered:

$$\Delta_n = E_n \tag{96}$$

and

$$\Delta_n = \left(E_{n-1}E_nE_{n+1}\right)^{1/3} \tag{97}$$

The two parameters ϵ and q are restricted to the intervals

$$q \in [0,1]$$

and

$$\epsilon \in [1,2]$$

In section 3.5 it will be shown that ϵ determines the form of a helicity-like conserved integral.

As in the 2D case, the 3 possible outcomes(L, G and N) are constructed to happen with certain probabilities. If $E_n > q\Delta_n$, $E_{n+1} > q(2-\epsilon)\Delta_n$ and $E_{n+2} > q(\epsilon-1)\Delta_n$, these probabilities are:

$$P_n^L(\mathbf{E}) = \begin{cases} \frac{1}{2}\frac{E_n}{\sqrt{E_{n+1}E_{n+2}}} & \text{, for } \frac{E_n}{\sqrt{E_{n+1}E_{n+2}}} < 2 \\ 1 & \text{, for } \frac{E_n}{\sqrt{E_{n+1}E_{n+2}}} 2 \end{cases} \tag{98}$$

$$P_n^G(\mathbf{E}) = \begin{cases} 1-\frac{1}{2}\frac{E_n}{\sqrt{E_{n+1}E_{n+2}}} & \text{, for } \frac{E_n}{\sqrt{E_{n+1}E_{n+2}}} < 2 \\ 0 & \text{, for } \frac{E_n}{\sqrt{E_{n+1}E_{n+2}}} 2 \end{cases} \tag{99}$$

$$P_n^N(\mathbf{E}) = 0 \tag{100}$$

Otherwise the probabilities are

$$P_n^L(\mathbf{E}) = 0 \tag{101}$$
$$P_n^G(\mathbf{E}) = 0 \tag{102}$$
$$P_n^N(\mathbf{E}) = 1 \tag{103}$$

If we once again let

$$X_n(t,\Delta t) = \begin{cases} 0 & \text{with probability } \left[1-\frac{\Delta t}{\tau_n(t)}\left(P_n^L(\mathbf{E})+P_n^G(\mathbf{E})\right)\right] \\ 1 & \text{with probability } \frac{\Delta t}{\tau_n(t)}P_n^L(\mathbf{E}) \\ -1 & \text{with probability } \frac{\Delta t}{\tau_n(t)}P_n^G(\mathbf{E}) \end{cases} \tag{104}$$

the stochastic dynamics of the 3D model can be described by

$$\begin{aligned} E_n(t+\Delta t) - E_n(t) = &- \left[\nu_1 k_n^2 \Delta t + \nu_2 k_n^{-2} \Delta t\right] E_n(t) - qX_n(t,\Delta t)\Delta_n(t) \\ &+ q(2-\epsilon)X_{n-1}(t,\Delta t)\Delta_{n-1}(t) \ + \ (\epsilon-1)(t)X_{n-2}(t,\Delta t)\Delta_{n-2}(t) \\ &+ \delta_{n,f} F \Delta t \end{aligned} \tag{105}$$

The l.h.s of equation (105) is the change in the energy on the n'th shell. The first term on the r.h.s is the energy lost to dissipation. The second term is the change in energy that comes about because of an eddy turnover on shell n. The following two terms describe the change in energy that comes about because of eddy turnovers on the two shells $n-1$ and $n-2$. Finally, the last term is a forcing that takes place on the f'th shell.

As boundary conditions, we require that:

$$\Delta N_{-1}^{ET}(t,\Delta t) = \Delta N_0^{ET}(t,\Delta t) = \Delta N_{N-1}^{ET}(t,\Delta t) = \Delta N_N^{ET}(t,\Delta t) = 0$$

The set of equation (105), the boundary conditions, and an initial condition, $\mathbf{E}(t=0) = \mathbf{E}_0$, specifies the stochastic process for the 3D model.

3.5 Conserved integrals

It was shown in section 2.1.2, that the NSE's for a 3D flow, conserve energy and helicity in the unforced, inviced limit. It was also shown that for a 2D flow, the NSE's have an extra conserved integral, called the enstrophy.
The two stochastic cascade models, presented above, have been constructed with conserved integrals that resemble the ones for the the NSE's.

We define the total energy of the models as the sum of the shell energies:

$$E = \sum_{1=n}^{N} E_n \tag{106}$$

As an analogue to helicity in the NSE's, we define the helicity of the 3D model as:

$$H = \sum_{1=n}^{N} H_n = \sum_{1}^{N} (-1)^n \left(\frac{1}{\epsilon-1}\right)^n E_n = \sum_{1=n}^{N} (-1)^n k_n^{\alpha} E_n x \tag{107}$$

where H_n is the local shell helicity, and we have introduced the parameter α:

$$\lambda^{\alpha} = \frac{1}{\epsilon-1} \tag{108}$$

Finally, we define the total enstrophy of the 2D model as:

$$Z = \sum_{1}^{N} Z_n = \sum_{1}^{N} \left(\frac{1}{\epsilon-1}\right)^n E_n = \sum_{1=n}^{N} k_n^{\alpha} E_n \tag{109}$$

where Z_n is the local shell enstrophy, and α is still defined by (108).

Notice, that similarly to the enstrophy and helicity of the NSE's, the enstrophy of the 2D model is a strictly positive quantity, whereas the helicity in the 3D model is not.

First, it will be shown that the 2D model conserves energy and enstrophy, in the unforced, inviscid limit. From equation (93), which describes the stochastic dynamics of the 2D model, without forcing or dissipation, we see that any change in energy and estrophy, is the result of a number of eddy turnovers, either loss or gain events. Therefore, we only need to show that a single eddy turnover conserves energy and enstrophy.
The change in the triad of shell energies (E_{n-1}, E_n, E_{n+1}) in a loss event on shell n, can be seen from equation (82) to be

$$\Delta E_{n-1} + \Delta E_n + \Delta E_{n+1} = q\frac{1}{\epsilon}\Delta_n - q\Delta_n + q\frac{\epsilon - 1}{\epsilon}\Delta_n = 0 \tag{110}$$

The change in the triad of shell enstrophies, (Z_{n-1}, Z_n, Z_{n+1}), in a loss event is:

$$\begin{aligned}\Delta Z_{n-1} + \Delta Z_n + \Delta Z_{n+1} &= q\frac{1}{\epsilon}k_{n-1}^{\alpha}\Delta_n - qk_n^{\alpha}\Delta_n + q\frac{\epsilon-1}{\epsilon}k_{n+1}^{\alpha}\Delta_n \\ &= qk_n^{\alpha}\Delta_n\Big(\frac{1}{\epsilon}\lambda^{-\alpha} - 1 + \frac{\epsilon-1}{\epsilon}\lambda^{\alpha}\Big) \\ &= qk_n^{\alpha}\Delta_n\Big(\frac{\epsilon-1}{\epsilon} - 1 + \frac{1}{\epsilon}\Big) \\ &= 0 \end{aligned} \tag{111}$$

Where we have used equation (82), (108) and (74).
Had we instead looked at the change in energy and enstrophy in a gain event, all the signs in the above expressions would be opposite, but the sums would remain zero. Equation (110) and (111) show that the 2D model conserves energy and enstrophy in the unforced, inviscid limit.

Now we show that the 3D model conserves energy and helicity in the unforced, inviscid limit. We look at the change in energy and helicity in a single eddy turnover.
From equation (95) we see that the total change in the triad of shell energies, (E_n, E_{n+1}, E_{n+2}), in a loss event on the n'th shell is

$$\Delta E_n + \Delta E_{n+1} + \Delta E_{n+2} = q(2-\epsilon)\Delta_n - q\Delta_n + q(\epsilon - 1)\Delta_n = 0 \tag{112}$$

The total change in the triad of shell helicities, (H_n, H_{n+1}, H_{n+2}), in a loss event on an even numbered shell is:

$$\begin{aligned}\Delta H_n + \Delta H_{n+1} + \Delta H_{n+2} &= -qk_n^{\alpha}\Delta_n - q(2-\epsilon)k_{n+1}^{\alpha}\Delta_n + q(\epsilon-1)k_{n+2}^{\alpha}\Delta_n \\ &= qk_n^{\alpha}\Delta_n\Big(-1 - (2-\epsilon)\lambda^{\alpha} + (\epsilon-1)\lambda^{2\alpha}\Big) \\ &= qk_n^{\alpha}\Delta_n\Big(-1 - \frac{2-\epsilon}{\epsilon-1} + \frac{\epsilon-1}{(\epsilon-1)^2}\Big) \\ &= 0 \end{aligned} \tag{113}$$

Had we looked at a gain event or an eddy turnover on an unequal shell, all the signs in the above expressions would have changed, but the net sum would still be zero. Equation (112) and (113) show that the 3D model conserves energy and helicity in the unforced, inviscid limit.

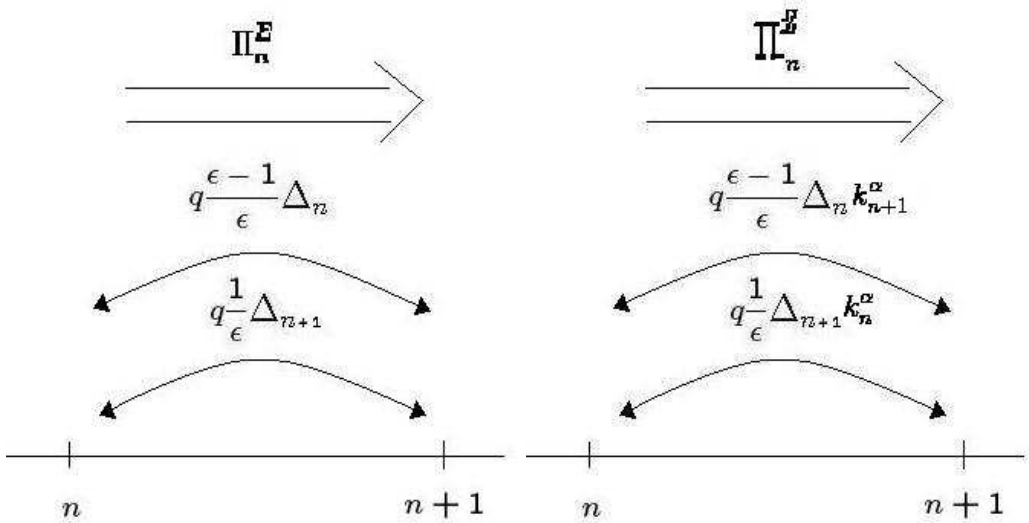

Figure 17: The figure shows the energy flux(left) and enstrophy flux(right) of the 2D model

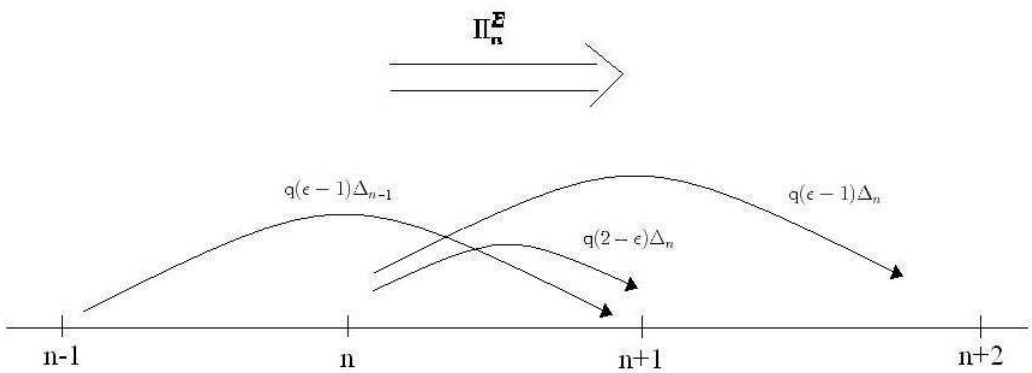

Figure 18: The figure shows the energy flux of the 3D model

3.6 Energy and enstrophy flux

As for the Navier-Stokes equations, we can define the energy and enstrophy flux of the models. The energy flux in the 2D model is defined as

$$\Pi_n^E(t,\Delta t) = q\frac{\epsilon-1}{\epsilon}X_n(t,\Delta t)\Delta_n(t) - q\frac{1}{\epsilon}X_{n+1}(t,\Delta t)\Delta_{n+1}(t) \tag{114}$$

This is the flux of energy from shell numbers lesser or equal to n, to higher shell numbers(see figure 17). The first term on the r.h.s is the contribution to the energy flux from eddy turnovers on shell n. The second term is the contribution from eddy turnovers on shell $n+1$. In a similar manner, we define the enstrophy flux for the 2D model as

$$\Pi_n^Z(t,\Delta t) = q\frac{\epsilon-1}{\epsilon}k_{n+1}^\alpha X_n(t,\Delta t)\Delta_n(t) - q\frac{1}{\epsilon}k_n^\alpha X_{n+1}(t,\Delta t)\Delta_{n+1}(t) \tag{115}$$

The energy flux in the 3D model is defined as

$$\Pi_n^E(t,\Delta t) = qX_n(t,\Delta t)\Delta_n(t) + q(\epsilon-1)X_{n-1}(t)\Delta_{n-1}(t,\Delta t) \tag{116}$$

In the 3D model, the contributions to the energy flux is made up of contributions from eddy turnovers on shells n and $n-1$(see figure 18).

Notice that similarly to the real NSE's only the non linear terms in the governing equations contribute to the energy flux. It should be mentioned, however, that the fluxes defined in equation (114), (115) and (116) are not strictly speaking fluxes, since they are not rates. They simply give the amount of energy or enstrophy moving to higher shell numbers in the small time interval Δt. The fluxes will be non zero only in discrete points in time, when eddy turnovers occur.

3.7 A steady state

Similarly to forced steady state turbulence for a real fluid described in section 2.2 and 2.3, we imagine that the models eventually reach a steady state, in which forcing is balanced by dissipation of energy and enstrophy(for the 2D model). Such a state will require the expectation values of the energy and enstrophy flux to be constant over a range of shells. With the pictures in figure 8 and 10 in mind, we imagine that the 3D model has a direct cascade of energy and the 2D model a Kraichman double cascade. In the 3D model, this will require the average energy flux to be constant and equal to the forcing:

$$\left\langle \Pi_n^E \right\rangle = F\Delta t \tag{117}$$

In the 2D model, it will require the average energy flux to constant and equal to minus the forcing

$$\left\langle \Pi_n^E \right\rangle = -F\Delta t \tag{118}$$

and the average enstrophy flux to be constant and equal to the enstrophy forcing

$$\left\langle \Pi_n^Z \right\rangle = k_f^\alpha F\Delta t \tag{119}$$

We may try to evaluate the 3 expectation values for the fluxes written above. Using the expressions (114), (115) and (116), we get

$$\begin{aligned}\left\langle \Pi_n^E \right\rangle =& q(2-\epsilon)\Big\langle X_n\Delta_n\Big\rangle(t) + q(\epsilon-1)\Big\langle X_n\Delta_n\Big\rangle(t) \\ &+ q(\epsilon-1)\Big\langle X_{n-1}\Delta_{n-1}\Big\rangle(t)\end{aligned} \tag{120}$$

$$\left\langle \Pi_n^E \right\rangle = q\frac{\epsilon-1}{\epsilon}\Big\langle X_n\Delta_n\Big\rangle(t) - q\frac{1}{\epsilon}\Big\langle X_{n+1}\Delta_{n+1}\Big\rangle(t) \tag{121}$$

$$\left\langle \Pi_n^Z \right\rangle = q\frac{\epsilon-1}{\epsilon}k_{n+1}^\alpha\Big\langle X_n\Delta_n\Big\rangle(t) - q\frac{1}{\epsilon}k_n^\alpha\Big\langle X_{n+1}\Delta_{n+1}\Big\rangle(t) \tag{122}$$

The above expression involve only expectation values of the kind $\Big\langle X_n\Delta_n\Big\rangle(t)$. This is the expectation value of the energy being lost or gained in an eddy turnover on the n'th shell. The expectation value will in general be time dependent. We may, however, assume that the stochastic process is first order stationary, so that $p(\mathbf{E},t) = p_{stat}(\mathbf{E})$, and try to

evaluate $\left\langle X_n \Delta_n \right\rangle$.

We look at the 2D model and use the probability function for the stochastic variable X_n, defined in equation (91). This is really a conditional probability, $p_n(x|\mathbf{E})$: It is the probabilities of different outcomes, given a certain configuration of shell energies.

Therefore, the expectation value $\left\langle X_n \Delta_n \right\rangle$ can be written

$$\left\langle X_n \Delta_n \right\rangle = \sum_{x=0,1,-1} \int_{R_+^N} d\mathbf{E} \;\; p_{stat}(\mathbf{E}) p_n(x|\mathbf{E}) x \Delta_n \tag{123}$$

Inserting the expression for $p_n(x|\mathbf{E})$, given in (91), we get

$$\begin{aligned} \left\langle X_n \Delta_n \right\rangle =& \Delta t k_n \int_\Omega d\mathbf{E} \;\; p_{stat}(\mathbf{E}) \Big[P_n^L(\mathbf{E}) - P_n^G(\mathbf{E}) \Big] \frac{\Delta_n}{\tau_n} \\ =& \Delta t k_n \int_\Omega d\mathbf{E} \;\; p_{stat}(\mathbf{E}) \Big[2 \min \Big(\frac{1}{2} \frac{E_n}{\sqrt{E_{n-1} E_{n-1}}}, 1 \Big) - 1 \Big] \sqrt{E_n} \Delta_n \end{aligned} \tag{124}$$

Where the integration is over $\Omega = \{\mathbf{E} \in R_+^N | E_n > q\Delta_n, E_{n-1} > \frac{q}{\epsilon}\Delta_n, E_{n+1} > q\frac{\epsilon-1}{\epsilon}\Delta_n\}$. This is the values of the shell energies for which both a loss and gain event are possible in the 2D model.

The expression (124), is as far as we can get without knowing the form of the stationary probability density $p_{stat}(\mathbf{E})$. One might have hoped that the steady state requirement, that the fluxes are constant in time and over the shells in the inertial range, would have led to some clear restrictions on the moments of $\mathbf{E}$.

In real turbulence, the 4/5-law is derived on the fact that the average energy flux must be constant in the inertial range. In the models, however, the assumption that the fluxes are constant, does not put any clear restrictions on any moments.

3.8 Structure functions and K41 scalings for the models

If we assume that in the forced steady state the models are first order stationary, the probability densities for the shell energies will be independent of time:

$$p(\mathbf{E}, t) = p_{stat}(\mathbf{E})$$

This means that all moments of the shell energies are time independent if they exist.

Using the assumptions of K41 theory, we can get the K41 scalings for the models. This is basically a repetition of the arguments presented in section 2.2.3 and 2.3.

The dimensions of the shell energy and the forcing are

$$[E_n] = \frac{length^2}{time^2}$$

$$[F] = \frac{length^2}{time^3}$$

If we assume that in the energy cascade the average shell energies are solely determined by the shell wave number and the average energy dissipation(equal to the forcing in steady state) the only possible scaling relation is

$$E_n \propto F^{2/3} k^{-2/3} \tag{125}$$

The dimensions of the shell enstrophy and the enstrophy forcing are

$$[Z_n = k_n E_n] = \frac{length^{2-\alpha}}{time^2}$$

$$\big[F_Z\big] = \big[f^\alpha F\big] = \frac{length^{2-\alpha}}{time^3}$$

If we assume that in the enstrophy cascade the average shell enstrophy is solely determined by the shell wave number and the average enstrophy dissipation(equal to the enstrophy forcing in steady state) the only possible scaling relation is

$$E(k) \propto (F_Z)^{2/3} k^{-2/3(\alpha+1)} \tag{126}$$

As an analogue to the structure functions in real turbulence we define the p'th order structure function for the cascade models as

$$S_p(n) = \Big\langle E_n^p \Big\rangle \tag{127}$$

The K41 predictions for the scaling exponents of the structure functions are $\zeta(p) = 2p/3$ in the energy cascade and $\zeta(p) = 2p(\alpha+1)/3$ in the enstrophy cascade.

3.9 Discussion of the two cascade models and a comparison with the Navier-Stokes equations

The two cascade models presented in this section are continuous time vector processes. They have the the Markov property(see appendix A.3), which can be seen from the stochastic difference equations (94) and (105), that govern the stochastic dynamics. These show that the outcome of the shell energies at time $t + \Delta t$, only depends on the value of the shell energies at time t.
The central idea of the models is that the energy is redistributed locally in k-space in eddy turnovers that occur according to a non homogeneous Poisson process, with rate parameter equal to the characteristic eddy turnover time. The energy is redistributed locally in k-space, in a way that conserves energy and helicity(3D model) or enstrophy(2D model). Only the local redistribution rules separate the two models, that are otherwise similar in structure.

The two cascade model are obviously toy models, and in that respect seem very far from the full NSE's. Still, it is interesting to compare the models to the differential equation for the spectral energy density given in equation (24). Obviously, the models are stochastic, whereas the NSE's are deterministic. The rate of change in energy in the equation for the spectral energy density involves triad interactions of the form

$$k v_{k'} v_{k-k'} v_{-k}$$

To compare with the models, we might look at the the rate of change in the expectation value of a shell energy, given a certain configuration of shell energies $\mathbf{E}(t) = \mathbf{E}'$:

$$\frac{1}{\Delta t}\Big\langle E_n(t+\Delta t) - E_n(t+\Delta t)|\mathbf{E}(t) = \mathbf{E}'\Big\rangle$$

This will involve terms of the form

$$\frac{1}{\Delta t}\Big\langle X_n(t,\Delta t)\Delta_n(t)|\ \mathbf{E}(t) = \mathbf{E}'\Big\rangle = \frac{1}{\Delta t}\sum_{x=0,1,-1} p_n(x|\mathbf{E}) x \Delta_n$$

The right hand side is just equation (123), with $p(\mathbf{E},t) = \delta\big(\mathbf{E}-\mathbf{E}'\big)$. Assuming that both a loss and a gain event is possible and that $E_n/\sqrt{E_{n-1}E_{n+1}} < 2$ for the energy configuration $\mathbf{E}'$, we evaluate the sum, using equation (91) for the 2D case:

$$\frac{1}{\Delta t}\Big\langle X_n(t,\Delta t)\Delta_n(t)|\mathbf{E}(t) = \mathbf{E}'\Big\rangle = \Big[P_n^L(\mathbf{E}) - P_n^G(\mathbf{E})\Big]\frac{\Delta_n}{\tau_n} \tag{128}$$

$$= \Big[\frac{E_n}{\sqrt{E_{n-1}E_{n+1}}} - 1\Big]k_n E_n \Delta_n \tag{129}$$

This expression depends on the triad of shell energies $\big(E_{n-1}, E_n, E_{n+1}\big)$, and like the triad interactions in the NSE's it has dimensions of wavenumber times energy to the power 3/2,.

Another point is that the NSE's govern the dynamics of the velocity field, whereas the dynamics of the cascade models only involve energy, one half the squared velocity. In the differential equation for the spectral energy density in the NSE's, the sign of the rate of change in the spectral energy, is determined by the signs of the triad of shell velocities,

$$k v_{k'} v_{k-k'} v_{-k}$$

The models are missing this sign. Instead, different signs in the rate of change of a shell energy, is made possible by the construction of loss and gain events(Determining the sign of X_n).

4 Simulations of the models

This section will describe the results of simulating the two cascade models. The 2D model has only been simulated with the triad interactions $\Delta_n = E_n$. The 3D model has been simulated with both types of triad interactions $\Delta_n = E_n$ and $\Delta_n = \left(E_{n-1}E_nE_{n+1}\right)^{1/3}$, but not as many simulations have been performed. The Simulations have been carried out in Matlab(The script for the 2D model can be seen in appendix A.4).

First some practical considerations regarding the simulations will be described. Then the simulations of the 2D and 3D models are analysed in separate sections.

4.1 Practical considerations regarding the simulations

The stochastic processes are simulated on a computer using the stochastic difference equations((94) for the 2D model and (105) for the 3D model), together with the the boundary conditions and an initial condition $\mathbf{E}(t=0) = \mathbf{E}_0$.
By generating random numbers, the computer produces a single realisation of the stochastic process

$$\left(\mathbf{E}_0, \mathbf{E}_1, \mathbf{E}_2, ...\mathbf{E}_M\right)$$

at equally spaced points in time

$$t_i = i\Delta t \quad , \text{ for } i = 0, 1, 2, .., M$$

In a simulation, it is important, that the time step, Δt, is small enough that the probability of a single eddy turnover can be approximated by

$$P\left[\Delta N_n^{ET}(t, \Delta t) = 1\right] = \frac{\Delta t}{\tau_n(t)} \tag{130}$$

$$P\left[\Delta N_n^{ET}(t, \Delta t) = 0\right] = 1 - \frac{\Delta t}{\tau_n(t)} \tag{131}$$

This is the case if $\frac{\Delta t}{\tau_n(t)} << 1$. We might require that

$$\frac{\Delta t}{\tau_n(t)} < u, \text{ for all } n, t \tag{132}$$

Where u is some upper limit that we set on the probability of an eddy turnover. The smaller we make u, the more precise the approximation made in (130) and (131).
However, this consideration has to be balanced with the concern that reducing the time step also reduces the length of simulations. A requirement on the length of a simulation might be that the number of eddy turnovers on all shells should be greater than some number

$$N_n^{ET} > N_{min}^{ET}$$

If the number of time steps in the simulation is M, then

$$N_n^{ET} \approx \frac{M\Delta t}{\langle \tau_n \rangle}$$

So we require that

$$M > \frac{N_{min}\langle\tau_n\rangle}{\Delta t} \text{ for all } n \tag{133}$$

Anticipating that the energy spectrum satisfies a power law $\langle E_n\rangle \propto k_n^{\gamma}$, the eddy turnover time will scale as $k_n^{-(1+\gamma/2)}$. For $\gamma > -2$, the eddy turnover time will be greatest at the smallest wave number. For $\gamma < -2$, it will be greatest at the largest wave number. If the scaling exist over a number of shells L(an inertial range), then the ratio of the largest and smallest eddy turnover will be

$$\tau_{max}/\tau_{min} = \lambda^{|L(1+\gamma/2)|} \tag{134}$$

Equation (132), sets a requirement on the smallest eddy turnover, τ_{min}, and equation (133) on the largest eddy turnover, τ_{max}. When we combine these requirements with the assumption of a power law scaling over an inertial range of L shells, expressed in equation (134), we get:

$$M > \frac{N_{min}^{ET}}{u}\lambda^{L|(1+\gamma/2)|} \tag{135}$$

So the required length of the simulation is proportional to N_{min}^{ET}, inversely proportional to u, and more importantly, grows exponentially with the number of shells. The last fact sets a limit on how many shells we can have in a simulation, and thereby, how long we can make the inertial range.

When performing the simulations, the parameters of the models can be varied. These parameters are the following:

- α: Determines the form of the enstrophy like, second inviscid invariant
- F: The forcing: Determines the energy and enstrophy input per time
- q: Determines the ratio of Δ_n being redistributed in an eddy turnover
- N: The number of shells
- λ: Determines the shell spacing trough $k_n = \lambda^n$
- f: The shell at which the forcing is taking place
- ν_1: The small scale viscosity
- ν_2: The large scale viscosity

4.2 Simulations of the 2D model with $\Delta_n = E_n$

The 2D model with the triad interactions $\Delta_n = E_n$, is the model that has been most thoroughly investigated. Simulations have been run to investigate the steady state behaviour of the the model, both when it is forced and viscid, and when it is unforced and inviscid.

ST run 1	N	λ	α	F	q	f	ν_1	ν_2
	25	2	3/2	1	0.1	13	$6.7725 \cdot 10^{-14}$	0.5307

Table 1: ST run 1

4.2.1 Forced, steady state simulations

In the first type of simulations that will be described, the model is forced at an intermediate shell, and eventually reaches a steady state in which forcing is balanced by energy and enstrophy dissipation.
Once the model has reached a steady state, it is allowed to run for a number of time steps. The time series generated in this steady state, is the basis of the analysis.
In the steady state, it is assumed that the process is weakly stationary. That is, the mean of the shell energies are time independent

$$< E_n > (i\Delta t) =< E_n >$$

and the autocovariance matrix of the shell energies only depend on the time difference

$$\begin{aligned}\Gamma_{n,n'}(i, i+j) =& \Big\langle \big(E_n(i\Delta t) - < E_n > \big)\big(E_{n'}((i+j)\Delta t) - < E_{n'} > \big)\Big\rangle \\ =& \Gamma_{n,n'}(j)\end{aligned}$$

The estimation of the mean, and autocovariance matrix from the the steady state runs has been done in the way described in section 2.5 on time series analysis. The mean of the energy and enstrophy fluxes have been estimated by sample averages.

An obvious question regarding this kind of experiment is: Will the model reach the same steady state for all initial conditions?
This has been tested by starting from different initial shell energies. Either from a state with a lot of redundant energy, or from a state with little or no energy. For the last type of initial condition, it takes a long time for the system to reach steady state, so this has only been tested once, and for a small number of shells. In all the cases that have been tested, the final steady state turns out to be independent of the initial condition.

4.2.2 Results from a single forced steady state simulation

We now look at results from a single steady state run(ST run 1), with the model parameters given in table 1. The figures 19 to 27 show results from this simulation.

Figure 19 and 20 show the normalised shell energy on shell 11 and 16 as a function of time, measured in average eddy turnover times. The time series have been generated in the steady state, and each figure shows the evolution of the shell energy for 3 different durations of time, corresponding to 100, 1000 and 10000 eddy turnovers.
It is not possible to distinguish between the time series from the two shells with the bare eye, except that the normalized energy on the 16'th shell seem to have a slightly greater variance. As mentioned, it is assumed In the analysis of the time series, that the process is weakly stationary in the steady state. Looking at figure 19 and 20, this seems plausible. The time series appear to have a constant mean and variance.

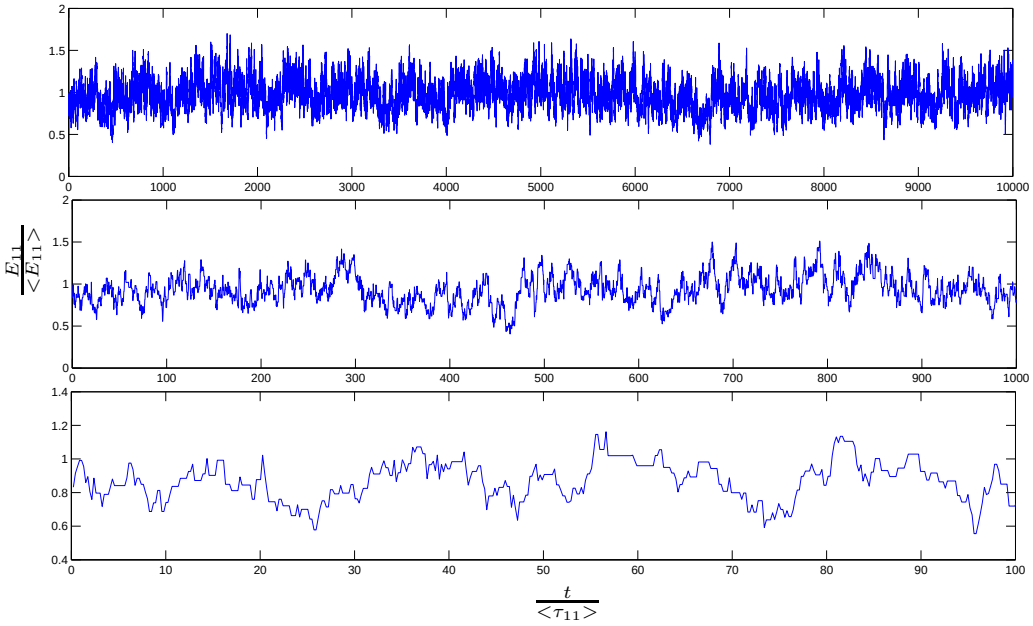

Figure 19: The figure shows 3 time series for the energy on the 11'th shell. The 3 time series show the same realisation of the stochastic process, but for different durations of time. The time axis have been rescaled by the average eddy turnover time, and the 3 time series correspond approximately to 100, 1000 and 10000 eddy turnovers. The shell energy has been normalized by the average shell energy

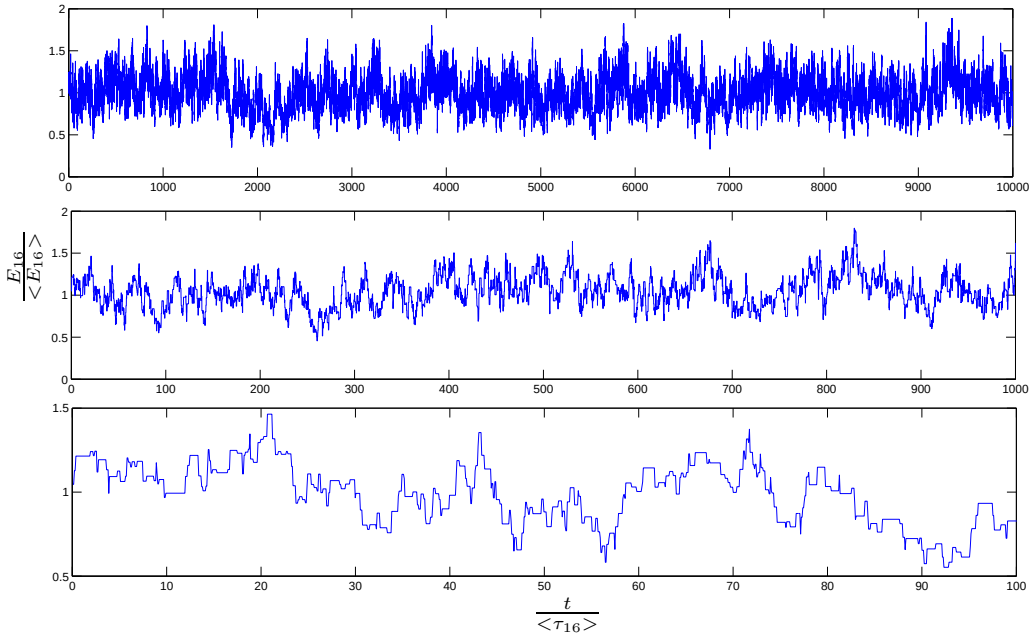

Figure 20: The figure shows 3 time series for the energy on the 16'th shell. The 3 time series show the same realisation of the stochastic process, but for different durations of time. The time axis have been rescaled by the average eddy turnover time, and the 3 time series correspond approximately to 100, 1000 and 10000 eddy turnovers. The shell energy has been normalized by the average shell energy

Figure 21 shows the average energy and enstrophy flux, normalised by the energy and enstrophy input. We see that the energy is dissipated at large length scales(small shell numbers) and enstrophy is dissipated at small length scales(large shell numbers). This fits the prediction of Kraichnans double cascade theory. The energy and enstrophy fluxes are constant over a range of shells, until dissipation sets in at shell 3(for energy) and shell

23(for enstrophy).

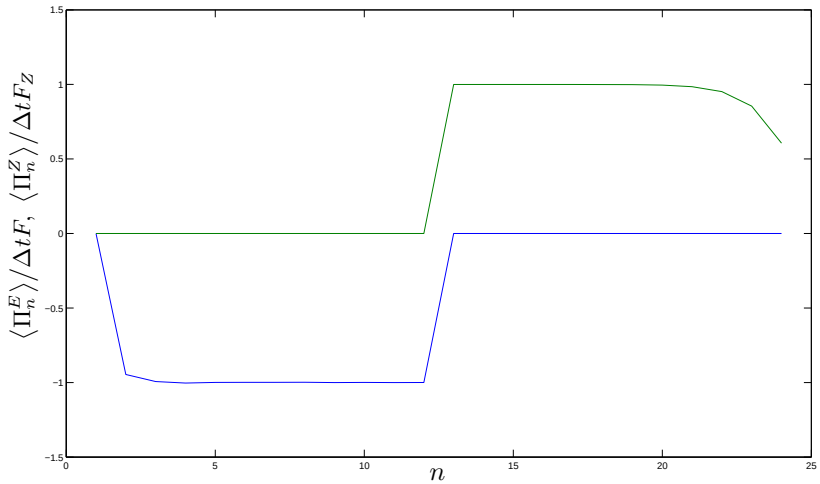

Figure 21: The average energy(blue) and enstrophy(green) flux, normalised by the average energy and enstrophy input

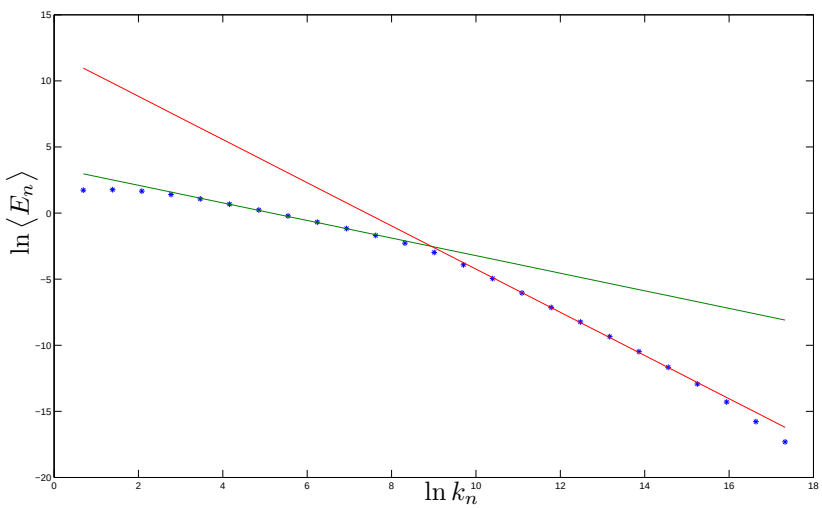

Figure 22: The energy spectrum of the model with $\alpha = 1.5$. The stars represent the the values of the average shell energies. The two straight lines are fitted lines, with slope -1.634(red) and -0.665(green)

Figure 22 shows the energy spectrum. The logarithm of the average shell energies, $< E_n >$, have been plotted against the logarithm of the shell wave numbers, k_n.
The stars represent the the values of the average shell energies. The errors on the estimations of the average shell energies are too small to show on the figure. The largest relative error, which is on the second shell, is 0.0273.
The two straight lines are fitted lines, with slopes $\gamma_Z = -1.634(-1.672, -1.595)$(red) and $\gamma_E = -0.665(-0.6943, -0.6357)$(green). These scaling exponents agree approximately with the kolmogorov predictions $\gamma_Z = -2(\alpha + 1)/3 = -5/3$ and $\gamma_E = -2/3$ described in section 3.8. The scaling exponent in the energy cascade agrees better than the scaling exponent in the enstrophy cascade.
The straight lines have been fitted with the unweighed least squares method, and the errors represent 95 proccent confidence intervals.

The two power law scalings of the energy spectrum persists over a range of shells, the two inertial ranges. It is over these ranges that the strait lines have been fitted. But how does one choose what the inertial range of the energy and enstrophy cascade is?
This has been done by visual inspection of the fluxes. If it is determined that the ranges over which the energy and enstrophy flux are constant, are $[\eta_E, \eta_E + 1, .., f]$ and $[f, f + 1, .., \eta_Z]$, respectively, then the inertial ranges are chosen to be $L_E = [\eta_E + 2, \eta_E + 3, .., f - 2]$ and $L_E = [f + 2, f + 3, .., \eta_Z - 2]$. This has been done the same way for all simulations, to try and assure some consistency when fitting to get the scaling exponents.

Figure 23 shows a double logarithmic plot of the variance of the shell energies versus the shell wave number. The stars represent the estimated shell variances. The shell variances are seen to also follow a power law in the two inertial ranges. The two straight lines are fitted lines, with slopes $-3.127(-3.203, -3.05)$(red) and $-1.319(-1.398, -1.241)$(green). The K41 scaling exponents for the variance are $-4(\alpha + 1)/3 = 10/3$ in the enstrophy cascade, and -3/4 in the energy cascade(the variance has the dimensions of the shell energy squared). Again, the scaling exponent in the energy cascade agrees better with the K41 scaling than the scaling exponent in the enstrophy cascade.

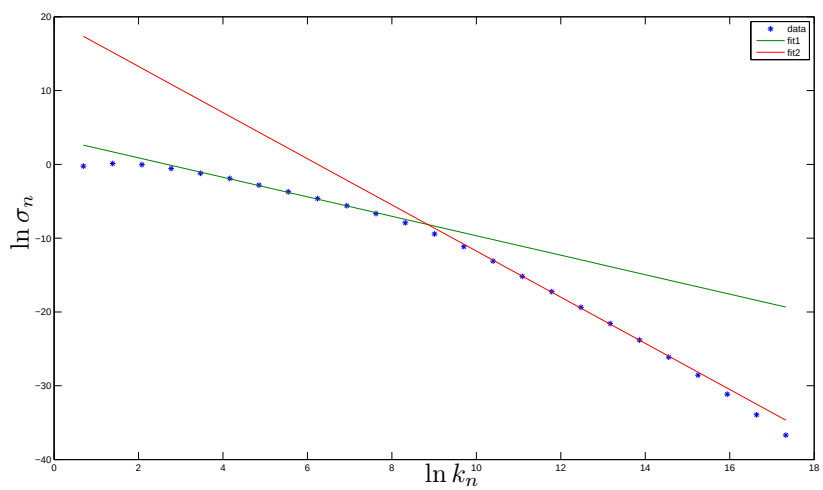

Figure 23: A double logarithmic plot of the variance of the shell energies vs. the shell wave number. The stars represent the estimated variances. The straight lines are fitted lines with slopes -3.127(red) and -1.319(green)

Figure 24 shows the autocorrelation function $\rho_{nn}(j)$ for the 18'th shell. It starts out at 1 and decays with time as one would expect. The correlation function is neither an exponentially decaying function or a power law, which has been checked by plotting it in a single and a double logarithmic plot. We can characterise the autocorrelation function by a characteristic correlation time, T^n_{corr}. This is chosen as the time it takes for the autocorrelation to be reduced by 1/2:

$$\rho_{nn}\big(T^n_{corr}\big) = 1/2$$

Figure 25 shows the logarithm of the characteristic correlation times for the different shell energies(blue stars), and the logarithm of the average eddy turnover time(green line), plotted against the logarithm of the shell wave number. All the average eddy turnover times have been shifted the same amount, so that the correspondence between

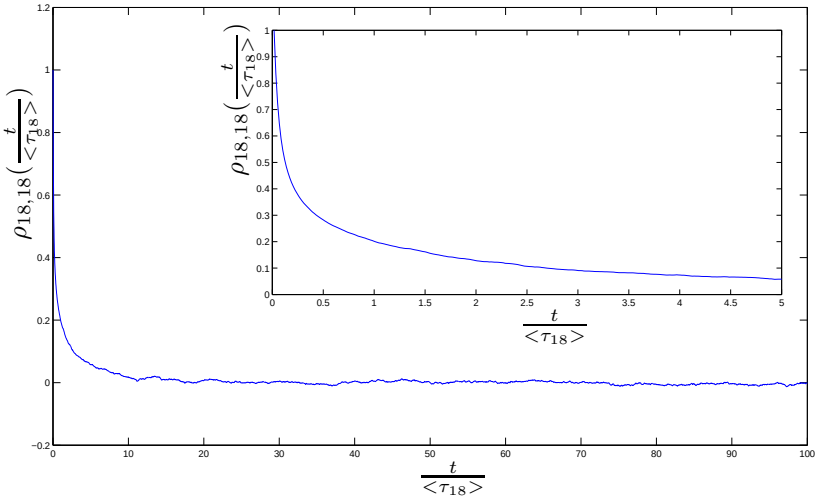

Figure 24: The figure shows the correlation function for the 18'th shell. The time axis have been rescaled by the average eddy turnover time. The small embedded figure shows the correlation function for the first 5 eddy turnover times

eddy turnover time and correlation time is easier to see.
In the energy cascade, the correlation time is seen to scale as the average eddy turnover time. In the enstrophy cascade, however, the correlation time does not scale with the eddy turnover time. Instead it looks constant over the shells and even grows towards the boundary.

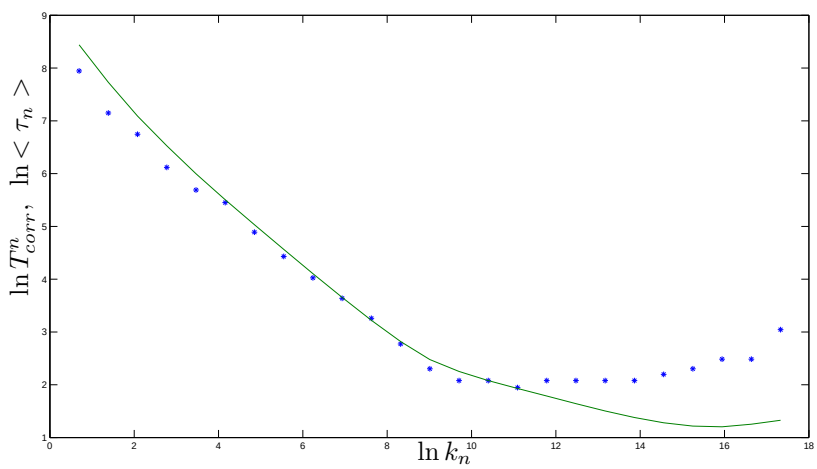

Figure 25: The figure shows a double logarithmic plot of the characteristic correlation time(the blue stars) of the shell energies vs. the wave number, and the average eddy turnover time(the green line) vs. the wave number

In figure 26 the autocorrelation functions in the two inertial ranges have been collapsed by rescaling the time axis by the characteristic correlation time. In the inertial range for energy(the shells 5 to 11) the rescaled correlation functions seem to overlap when the correlation is between 1 and 0.3. This indicates that the correlation functions have the form

$$\rho_{nn}(t) = f\left(t/T^n_{corr}\right)$$

Where f is a function that is independent of the shell number. When the correlation becomes less than 0.3, the overlap of the rescaled autocorrelation functions is not as

convincing. This may be because the statistics becomes less good for longer times.
In the inertial range for enstrophy(the shells 15 to 21), the correlation functions do not overlap convincingly.

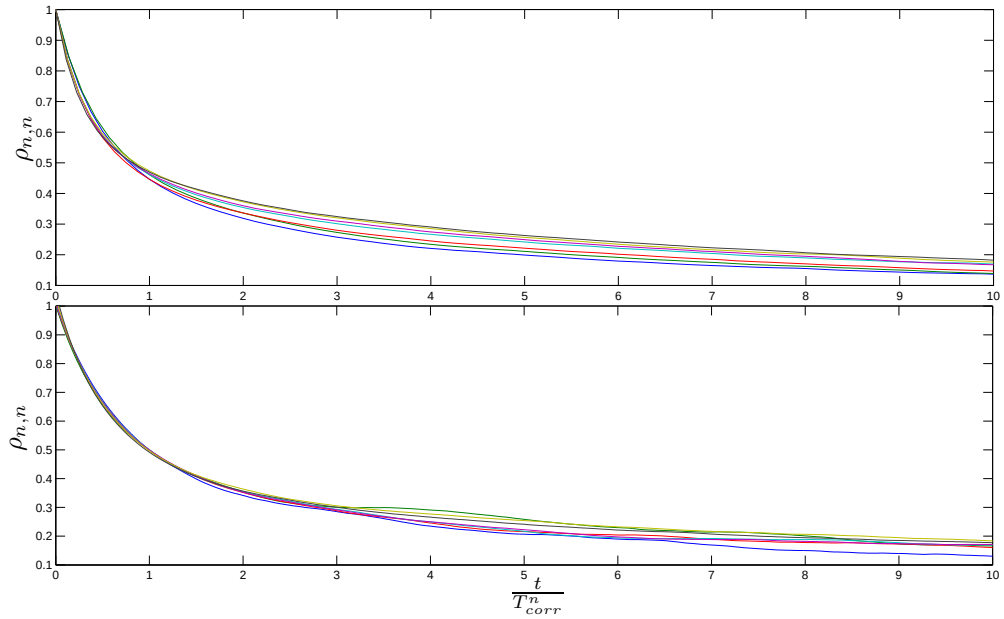

Figure 26: The figure shows the correlation functions for the 5'th to the 11'th shell(bottom) and the 15'th to the 21'th shell(top). The correlation functions have been collapsed by rescaling the time by the characteristic correlation time T^n_{corr}

Finally we look at the correlations between the shell energies. In figure 27 we show the 8'th(left) and 18'th(right) column of the correlation matrix. That is, the correlation between the 8'th(18'th) shell with itself and the rest of the shells. The two columns of the correlation matrix are very representative for the rest of the columns. We see that the correlations are local in k-space: The shells are only significantly correlated to the four nearest neighbours. In the energy cascade, the shell energies are negatively correlated to their nearest neighbours. In the enstrophy cascade, they are positively correlated to their nearest neighbours and negatively correlated to their next to nearest neighbours.

The results described above for a single simulation(ST run 1) are characteristic for many of the forced steady state simulations that have been carried out. For a wide range of the model parameters, the simulations agree very well with the Kraichnan double cascade picture. They show a direct cascade of enstrophy and an indirect cascade of energy. In the inertial range for energy, the energy spectrum scales as a power law with a scaling exponent, γ_E, that is approximately equal to -2/3.
In the inertial range for enstrophy, the energy spectrum also scales as a power law, but with a different exponent, γ_Z, that is approximately equal to $-2(\alpha+1)/3$. The variance of the shell energies have scaling exponents approximately equal to -4/3 in the energy cascade and $-2(\alpha+1)/3$ in the enstrophy cascade. These are the scalings predicted by K41 theory(see section 3.8).

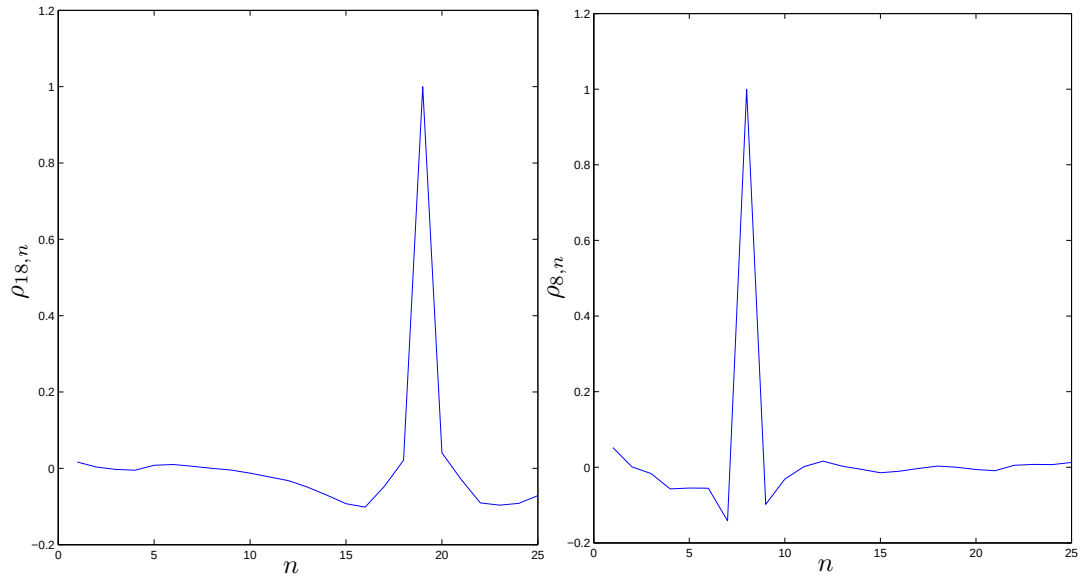

Figure 27: The figures show two columns of the correlation matrix for the shell energies, $\rho_{n,n'}$. The figure on the left shows the correlation between the 18'th shell and the rest. The figure on the right shows the correlation between the 8'th shell and the rest

4.2.3 Variation of α

To test the dependence of the scaling of the energy spectrum on the enstrophy-like inviscid invariant, simulations have been carried out for different values of α.
Figure 28 shows the scaling exponents γ_E(green stars) and γ_Z(blue stars) of the energy spectrum for a set of 5 simulations with different values of α(1, 3/2, 2, 5/2, and 3). The parameters N, λ, F and q are the same as in the simulation ST run 1(see table 1) for all 5 simulations. The small and large scale viscosities $\nu 1$ and $\nu 2$ have been chosen for each simulation, so as to get the longest possible inertial ranges for energy and enstrophy, while not having any boundary effects(build up of energy or enstrophy on the boundary shells). The error bars in the plot indicate the 95 proccent confidence intervals for the fits. The two straight lines represent the kolmogorov prediction for the scaling exponents. The results of the simulations agrees quite well with the Kolmogorov scaling theory.

The value $\alpha = 2$ is of special interest. The eddy turnover time in the enstrophy cascade scales as

$$\langle \tau_n \rangle = \frac{1}{k_n \sqrt{\langle E_n \rangle}} \propto k_n^{2(alp+1)/3-1}$$

So for values of alpha greater than 2, the eddy turnover time will grow with the shell number in the enstrophy cascade. One might have imagined that when the eddy turnover time grew with shell number, the enstrophy would have time to equipartition and we would instead see the scaling $E_n \propto k_n^{alpha/2}$, corresponding to statistical equilibrium for the enstrophy. This has been shown by [*Ditlevsen and Mogensen*, 1996] to be the case for the GOY shell model, mentioned in the introduction, where there is a crossover from cascade to equipartition at $\alpha = 2$.

Figure 29 shows a collapse of the energy spectrums for the 5 different values of α. The logarithm of the rescaled energy spectrums $\epsilon^{-2} < E_n >$, have been plotted against the logarithm of the shell wave numbers. ϵ is related to α through equation (108). The

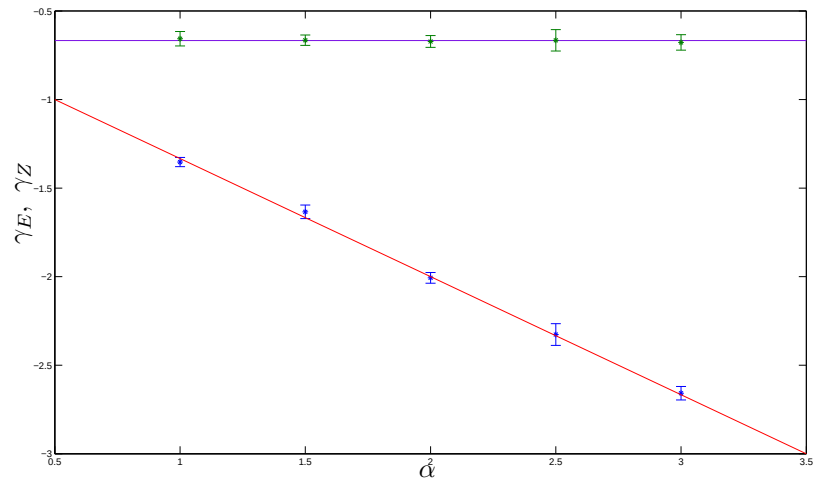

Figure 28: The figure shows the fitted scaling exponents γ_E(green stars) and γ_Z(blue stars) of the energy spectrum, for a set of 5 simulations with different values of α(1, 3/2, 2, 5/2, and 3). The error bars represent the 95 percent confidence intervals of the fits. The two straight lines represent the kolmogorov prediction for the scaling exponents

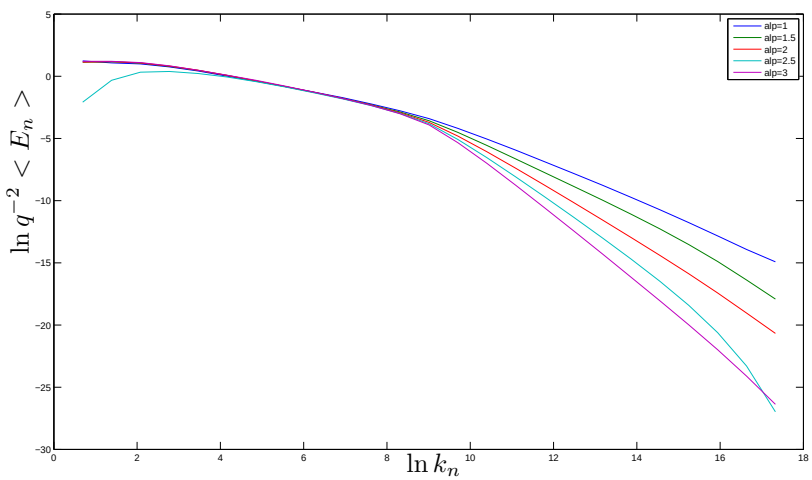

Figure 29: The figure shows a collapse of the energy spectrums for 5 different values of α(1, 3/2, 2, 5/2, and 3). The logarithm of the rescaled energy spectrums $\epsilon^{-2} < E_n >$, have been plotted against the logarithm of the shell wave numbers.

overlap of the energy spectrums in the the inverse energy cascade, indicates that the energy spectrum scales as ϵ^2.

The 5 simulation with different values of α described above all have $\alpha \geq 1/2$. It it interesting to know how the model behaves when $\alpha \to 0$. In this limit the enstrophy and energy become the same quantity, and the model only has one conserved integral. However, in simulations that have been carried out with α less or equal to 1/2 the model has not settled in to a weakly stationary steady state. It is not clear whether the the model will eventually reach such a steady state in which the shell energies are weakly stationary. For simulations with $\alpha = 1/2$, the shell energies in the enstrophy cascade seem to be weakly stationary, and the scaling in this cascade agrees well with the K41 scaling prediction. In the energy cascade, the shell energies do not seem to reach a weakly stationary state. This manifests itself in the fact that the estimations of the shell energies by sample averages, varies when one considers different periods of estimation.

ST run 2	N	λ	α	F	q	f	ν_1	ν_2
	25	2	3/2	1	0.1	22	$1.5324e \cdot 10^-12$	0.5307
ST run 3	N	λ	α	F	q	f	ν_1	ν_2
	25	2	3/2	1	0.1	4	$2.993 \cdot 10^-15$	0.5307

Table 2: ST run 2 and 3

In the simulations performed for $\alpha = 0$, none of the shell energies reach a weakly stationary state.

4.2.4 Simulations with longer energy and esntrophy cascades

One might be concerned with the relatively short inertial ranges that have been used to get the scaling exponents. The scaling exponents plotted in figure 28 have been fitted over 5 to 6 shells in most cases. To test whether the scaling of the energy spectrums hold for longer inertial ranges, simulations with longer energy and enstrophy cascades have been carried out. In one simulation(ST run 2) the model is forced forced at shell 4, to have a long energy cascade. In another simulation(ST run 3)it is forced forced at shell 22, to have a long enstrophy cascade. The rest of the model parameters for the two runs are shown table 2.

Figure 30 shows the fluxes and energy spectrum for the model forced at shell 4(ST run 3). The figure on the top shows the average energy and enstrophy flux, normalised by the energy and enstrophy input. We see that the enstrophy is cascaded to large shell numbers, where it is dissipated, and that energy is dissipated at small shell numbers. The inertial range for the enstrophy spans 14 shells(6 to 20).
The figure on the bottom shows the energy spectrum for the simulation. The logarithm of the average shell energies, $< E_n >$, have been plotted against the logarithm of the shell wave numbers, k_n.
The stars represent the the values of the average shell energies. The straight line is a fitted line, with slope $\gamma_Z = -1.671(-1.678, -1.663)$. This scaling exponents agrees very well with the Kolmogorov prediction $\gamma_Z = -2(\alpha + 1)/3 = -5/3$.

Figure 4.2.4 shows the fluxes and energy spectrum for the model forced at shell 22(ST run 2). Again, the figure on the top shows the average energy and enstrophy flux, normalised by the energy and enstrophy input. We see that the energy is cascaded to small shell numbers, where it is dissipated, and that enstrophy is dissipated at large shell numbers. The inertial range for the energy spans 9 shells(11 to 20).
The figure on the bottom shows the energy spectrum for the simulation. The logarithm of the average shell energies, $< E_n >$, have been plotted against the logarithm of the shell wave numbers, k_n.
The stars represent the the values of the average shell energies. The straight line is a fitted line, with slope $\gamma_E = -0.6661(-0.6756, -0.6567)$. This scaling exponents, again agrees very well with the Kolmogorov prediction $\gamma_E = -2/3$.

The confidence interval for the fitted scaling exponents for the two simulations are much narrower than in the simulations described earlier, because the inertial ranges are much longer. The inertial range for the energy would have been longer, had the simulation been run for a longer time. The shell energies on the small shell numbers have

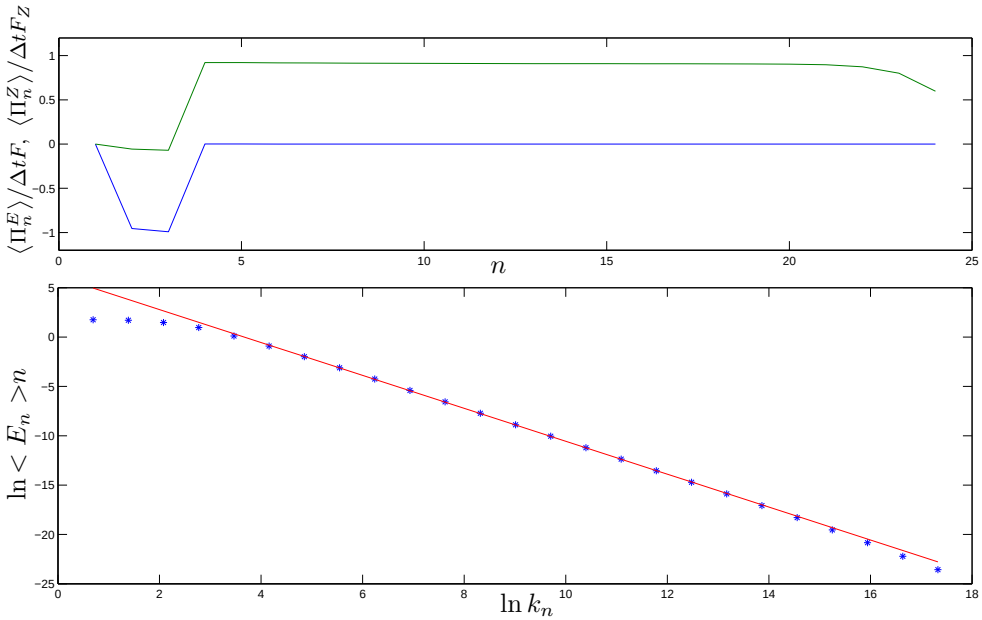

Figure 30: The figure shows results from a simulation where the model is forced at shell 4(ST run 3). The figure on the top shows the average energy and enstrophy flux, normalised by the energy and enstrophy input. The figure on the bottom shows the logarithm of the average shell energies, $< E_n >$ versus the logarithm of the shell wave numbers, k_n. The straight line is a fitted line, with slope $\gamma_Z = -1.671(-1.678, -1.663)$.

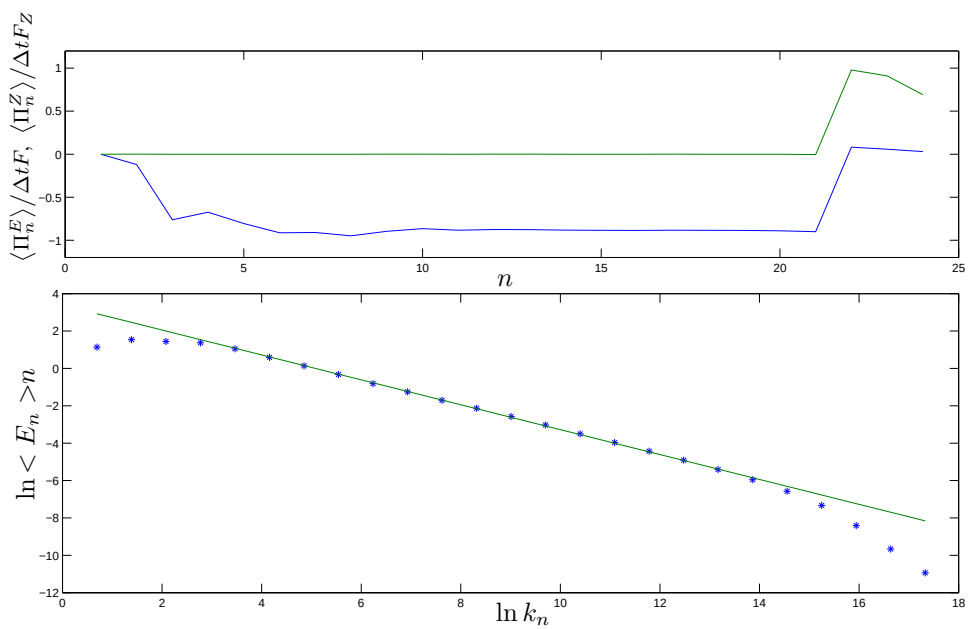

and energy spectrum for long energy cascade]The figure shows results from a simulation where the model is forced at shell 22(ST run 2). The figure on the left shows the shows the average energy and enstrophy flux, normalised by the energy and enstrophy input. The figure on the right shows the logarithm of the average shell energies, $< E_n >$ versus the logarithm of the shell wave numbers, k_n. The straight line is a fitted line, with slope $\gamma_E = -0.6661(-0.6756, -0.6567)$.

not had sufficient time to reach the steady state, and this is why the average energy flux looks a bit suspicious for small shell numbers.

ST run 4	N	λ	α	F	q	f	ν_1	ν_2
	25	2	5/2	1,2,3	0.1	13	$1.5324e \cdot 10^-12$	0.5307

Table 3: ST run 4

4.2.5 Variation of F and q

Kolmogorovs scaling theory also predicts that the energy spectrum scales with the forcing as $F^{2/3}$. To test if the models behave the same way, 3 simulations have been run with different forcings($F = 1, 2, 3$). The values of the rest of the model parameters are shown in table 3. Figure 31 shows the energy spectrums for these 3 simulations, rescaled by $F^{-2/3}$. The 3 energy spectrums clearly overlap, strongly indicating that the steady state energy spectrum of the model scales with the forcing as $F^{2/3}$, as predicted by Kolmogorov scaling theory.

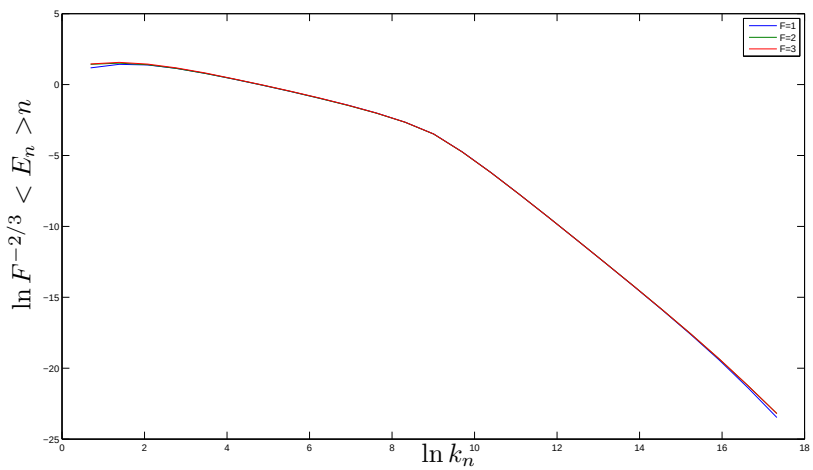

Figure 31: The figure shows a collapse of the energy spectrums for different forcings(F=1,2,3). The logarithm of the rescaled energy spectrums $F^{-2/3} < E_n >$, have been plotted against the logarithm of the shell wave numbers.

Now we look at 3 simulations for varying values of the parameter q(0.1, 0.15, and 0,2). Again, the rest of the parameters are kept the same as in the simulation ST run 1. Figure 32 shows the energy spectrum of the 3 simulations rescaled by q. The energy spectrums clearly overlap, strongly indicating that the energy spectrum scales as q^{-1}.

4.2.6 Distribution functions and intermittency

If we assume that in the steady state the 2D model is not only weakly stationary, but also first order stationary, the probability densities for the shell energies will be independent of time:

$$p(\mathbf{E}, t) = p_{stat}(\mathbf{E})$$

The probability density for a particular shell is then given by

$$p_n(E) = \int p_{stat}(\mathbf{E}) \prod_{n' \neq n} dE_{n'}$$

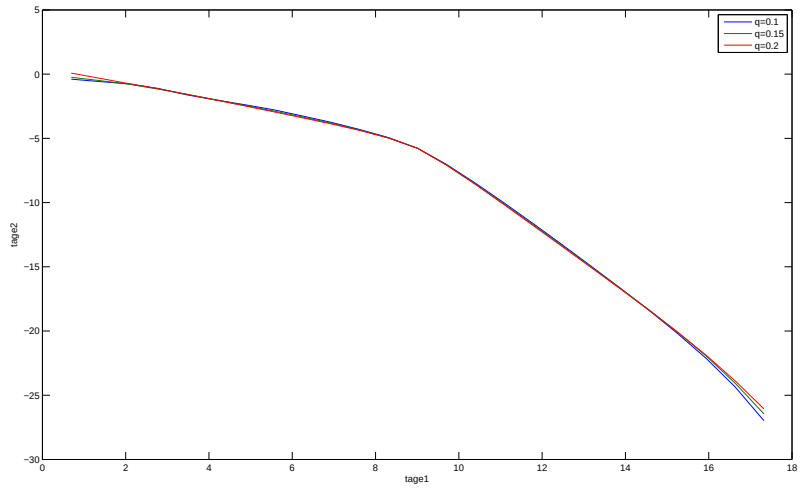

Figure 32: The figure shows a collapse of the energy spectrums for different values of the parameter qforcings(q=0.1, 0.15, 0.2). The logarithm of the rescaled energy spectrums $q < E_n >$, have been plotted against the logarithm of the shell wave numbers.

Figure 37 shows the probability densities for 4 different shells(5, 10, 17 and 20) for the simulation ST run 1, estimated on the basis of 4 different time series of the same length. The probability densities have been estimated by way of histograms. The 4 different estimates seem to overlap, indicating that the assumption of first order stationarity is reasonable.

As is shown in figure 34, the probability densities for the shell energies fit very well to gamma distributions. The figure shows the probability densities(blue lines) and the fitted gamma distributions(green lines) for the energies on 6 different shells(5,10,14,17,19 and 23), estimated from the simulation ST run 1.

Gamma distributions have the form:

$$p_n(E) = E^{a_n - 1} \frac{e^{E/b_{b_n}}}{b_n^{a_n} \Gamma(a_n)} \tag{136}$$

where $\Gamma(x) = \int_0^\infty \; t^{x-1} e^{-t} dt$ is the gamma function. The distribution has two parameters: The shape parameter, a_n, and the scale parameter, b_n. The parameters have been indexed by shell number, since they will be different for different shell energies. Gamma distributions are often encountered in waiting time problems, because the time it takes for a specific number of events to occur in a Poisson process is distributed according to a gamma distribution. It is therefore not completely surprising that the probability densities agree well with gamma distributions, since the Poisson process lies at the core of the models.

Figure 35 shows the scale and shape parameter of the fitted gamma distributions. The top figure shows the logarithm of the scale parameter plotted against the logarithm of the shell wave number. Two straight lines with slope $-2/3$ and $-2(\alpha+1)/3$ have been included in the plot to indicate that the scale parameter scales approximately as $k_n^{-2/3}$ in the inertial range for energy and $k_n^{-2(\alpha+1)/3}$ in the inertial range for enstrophy.
The bottom figure show the shape parameter plotted against the shell number. The shape parameter is seen to be roughly constant over the shells.
It can be shown from the properties of the gamma distribution that if the shape parameter

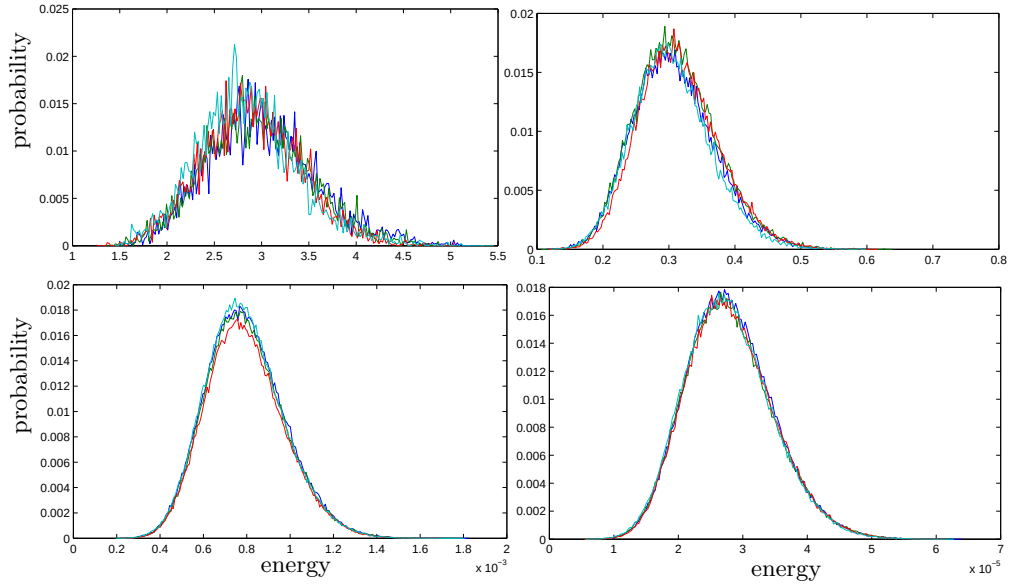

Figure 33: The figure shows the probability densities for energies on 4 different shells, estimated by four different time series of the same length. The four colours represent the four different estimation. The shells are 5(top left), 10(top right), 17(bottom left) and 20(bottom right)

is constant over the shells and the scale parameter has the scaling exponent γ, the moments of the shell energy will scale as:

$$S_p(n) = \left\langle E_n^p \right\rangle \propto b_n^p \propto k_n^{p\gamma}$$

This means that if the approximate observations of the scale and shape parameters given above where strictly true , there would be no intermittency corrections to the scaling exponents of the structure functions.

In figure 36 the estimated scaling exponents for the structure functions, $\zeta(p)$, have been plotted as a function of p. The left figure show the scaling exponents in the inertial range for energy, calculated from the simulation ST run 2. The right figure shows the scaling exponents in the inertial range for enstrophy, calculated from the simulation ST run 3. These two simulations have been chosen, because they have the longest inertial ranges for energy and enstrophy respectively. The green lines in the figures are the K41 predictions. The estimated scaling exponents clearly overlap with the K41 predictions, indicating that the model does not have any intermittency corrections.

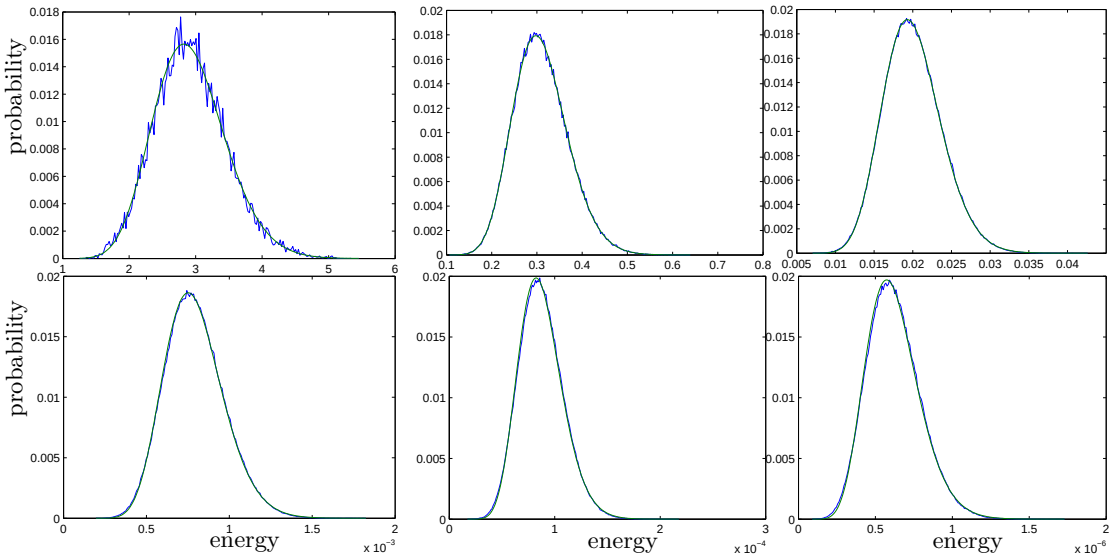

Figure 34: The figure shows the estimated probability densities(blue lines) and fitted gamma distributions(green lines) for energies on 6 different shells(5,10,14,17,19 and 23). The figures are ordered by growing shell number, so that shell 5 is in the top left corner and shell 23 is in the bottom right corner.

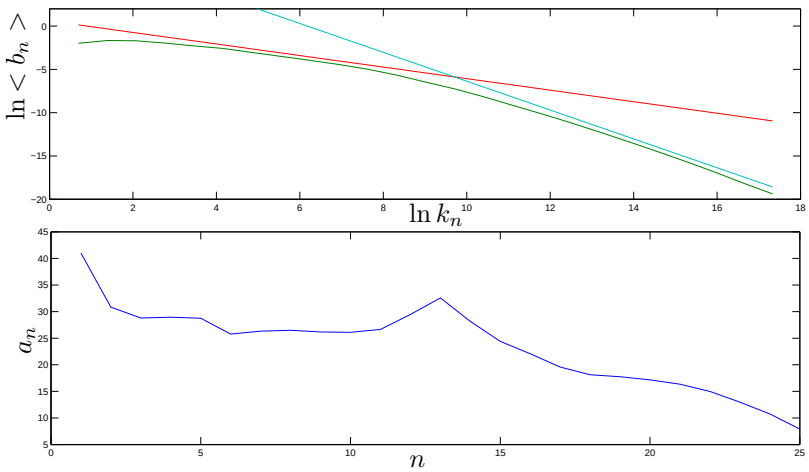

Figure 35: The figure shows the fitted parameters for the gamma distributions. The top figure shows the logarithm of the fitted scale parameter versus the logarithm of the shell wave number. Two straight lines with slope $-2/3$ and $-2(\alpha+1)/3$ have been included in the plot The bottom figure shows the fitted shape pararameter as a function of shell number.

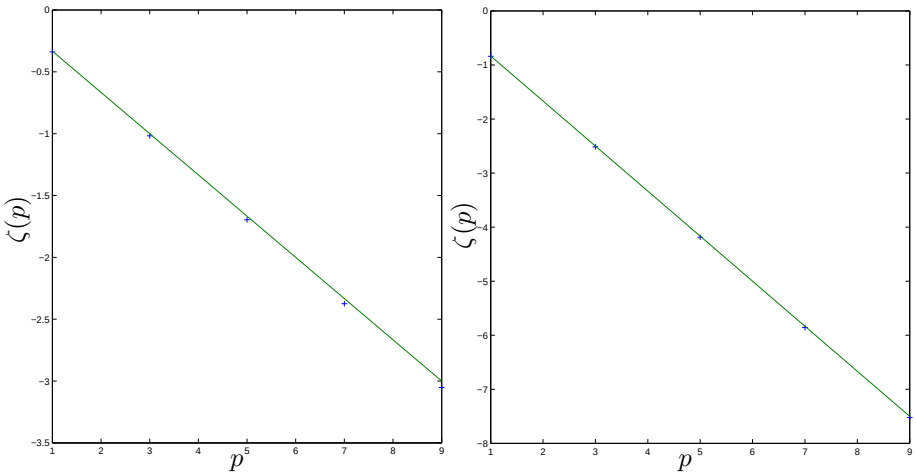

Figure 36: The figure shows the scaling exponents of the structure functions as a function of the order of the structure functions. The left hand figure shows the scaling exponents in the energy cascade and the right hand figure shows the scaling exponents in the enstrophy cascade. The green lines show the K41 prediction for the scaling exponents

ST run 5	N	λ	α	F	q	ν_1	ν_2
	15	2	3/2	0	0.1	0	0

Table 4: ST run 5

4.2.7 simulation of the unforced, inviced model

Simulation have been performed to see how the unforced, inviscid model behaves. As in the forced steady state runs, the model is allowed to settle in to a weakly stationary state, and it is from the time series generated in this state that the average values have been estimated.

Figure 37 shows the energy spectrum of a simulation of the model with the parameters given in table 4. The number of shells has been chosen smaller than in the forced, viscid simulations, because the unforced, inviscid model takes a very long time to reach the weakly stationary state. One might have hoped that the energy spectrum would have shown an equipartition of either energy or enstrophy, corresponding to an energy spectrum that scaled as $E_n = constant$ or $E_n \propto k_n^{\alpha/2}$. This is not the case. Instead the energy spectrum seems to scale as $2(\alpha+1)/3$, corresponding to the K41 prediction for the enstrophy cascade. This has been indicated by including a line with the slope $2(\alpha+1)/3$ in the plot. We also see that energy has build up in the high wave numbers, towards the boundary shell, which is not very physically reasonable.

4.2.8 Conclusions drawn from the simulations of the 2D model

We now list the main conclusions that can be drawn from the simulations of the 2D model. As has been shown, when α is greater than 1/2, the model reaches a weakly stationary steady state in which it has a double cascade similar to the one predicted by Kraichnan for 2D turbulence. The energy is cascaded to large length scales in an inverse cascade and enstrophy is cascaded to small length scales in a direct cascade. The scaling of the energy spectrum in the two cascades agree very well with the K41 prediction. If we collect the results of the simulations where the quantity q, the forcing(F), and α have been varied,

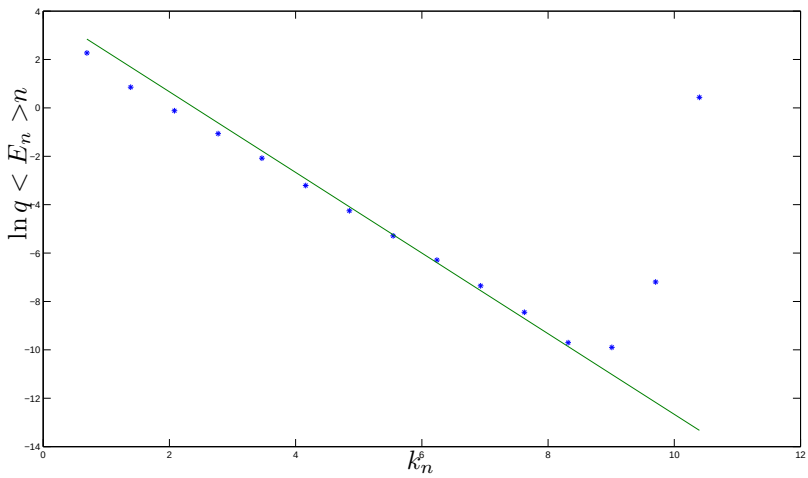

Figure 37: The figure shows the logarithm of the average shell energy(blue stars) plotted against the logarithm of the shell wave number for the unforced, inviscid model with $\alpha = 1.5$. A straight line with slope $2(\alpha+1)/3$ has been included in the plot

the energy spectrum is seen to have a form

$$\left\langle E_n \right\rangle \propto \frac{F^{2/3}\epsilon^2}{q} k_n^{\gamma_{E,Z}}$$

Where the scaling exponent in the inverse cascade of energy is $\gamma_E = -2/3$ and the scaling exponent in the direct enstrophy cascade is $\gamma_Z = -2(\alpha+1)/3$.

It was also shown from the simulations, that the probability densities for the shell energies agree very well with gamma distributions, and the structure functions do not show any intermittency corrections to the scaling exponents.

ST run 6	Δ_n	N	λ	α	F	q	f	ν_1	ν_2
	E_n	20	2	3/2	1	0.1	4	$7.4066 \cdot 10^{-9}$	0
ST run 7	Δ_n	N	λ	α	F	q	f	ν_1	ν_2
	E_n	20	2	5/2	1	0.1	4	$9.4450 \cdot 10^{-9}$	0

Table 5: ST run 6 and 7

ST run 8	Δ_n	N	λ	α	F	q	f	ν_1	ν_2
	$\left(E_{n-1}E_nE_{n+1}\right)^{1/3}$	20	2	3/2	1	0.1	4	$5.2550 \cdot 10^{-9}$	0
ST run 9	Δ_n	N	λ	α	F	q	f	ν_1	ν_2
	$\left(E_{n-1}E_nE_{n+1}\right)^{1/3}$	20	2	5/2	1	0.1	4	$5.0035 \cdot 10^{-10}$	0

Table 6: ST run 8 and 9

4.3 Simulations of the 3D model

This section will describe the results of simulating the 3D model. Not as many simulations have been carried out as for the 2D model, and the analysis of the results will not be thorough.

Four simulations have been carried out, two with the triad interactions $\Delta_n = E_n$ and two with $\Delta_n = \left(E_{n-1}E_nE_{n+1}\right)^{1/3}$. The model parameters for the 4 simulations are shown in table 5 and 6.

All 4 simulations show a forward cascade of energy as in the Richardson picture of 3D turbulence. There is an inertial range for energy over which the flux of energy is constant and equal to the forcing. The energy spectrum of all 4 simulations agree well with the K41 prediction that the shell energy scales as $k_n^{-2/3}$. The scaling exponents for the 4 simulations have been found to be:

- ST run 6: -0.676 (-0.6807, -0.6713)
- ST run 7: -0.6757 (-0.6817, -0.6696)
- ST run 8: -0.669 (-0.6774, -0.6606)
- ST run 9: -0.672 (-0.6794, -0.6646)

Where the errors represent 95 proccent confidence intervals on the fits.
Figure 38 and 39 show the energy spectrum and the normalized energy flux of the simulations ST run 6 and ST run 8. ST run 6 is a simulations with the triad interactions $\Delta_n = E_n$ and ST run 8 is a simulation with triad interaction $\Delta_n = \left(E_{n-1}E_nE_{n+1}\right)^{1/3}$. The energy spectrum of the two simulations are very similar.

In the following we only consider results from the simulation ST run 6.
Figure 40 shows the correlation function of the 12th shell energy(left) and the characteristic correlation times for the different shells(right). The characteristic correlation times are defined as was done previously for the simulations of the 2D model. As was the case in the 2D model, the correlation function(shown on the left hand figure) is neither an exponentially decaying function nor a power law. This has been checked by plotting it on a single and double logarithmic plot.

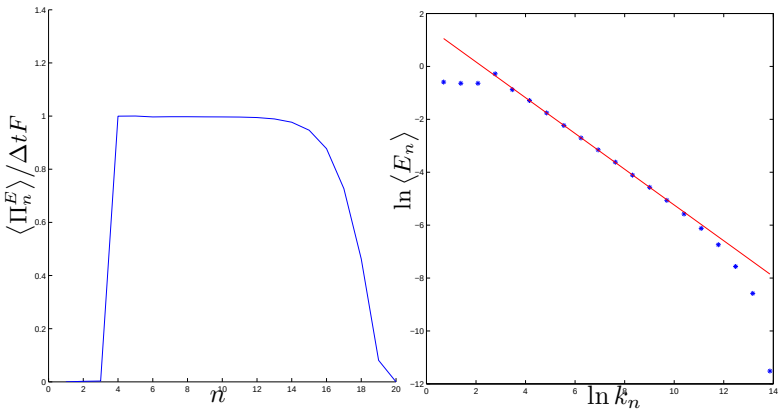

Figure 38: The figure shows the normalised energy flux(left) and the energy spectrum(right) for the simulation ST run 6

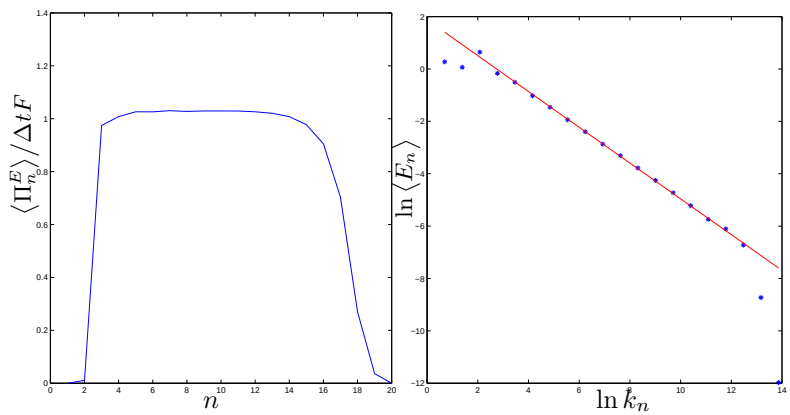

Figure 39: The figure shows the normalised energy flux(left) and the energy spectrum(right) for the simulation ST run 8

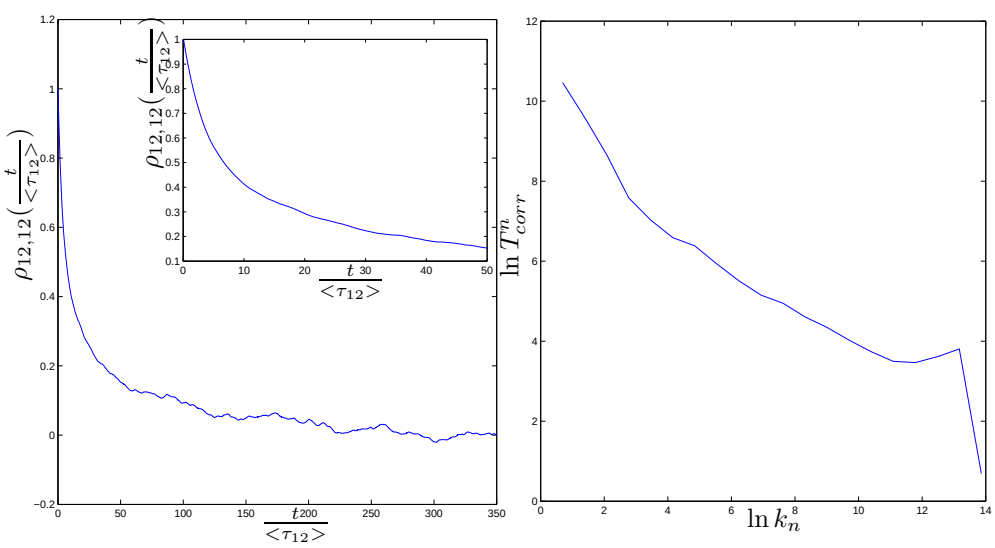

Figure 40: The left hand figure shows the autocorrelation function for the 12th shell. The time axis have been rescaled by the average eddy turnover time. The small embedded figure shows the correlation function for the first 50 eddy turnover times. The right hand figure shows a double logarithmic plot of the characteristic correlation time of the shell energies vs. the wave number. The results are from the simulations ST run 6

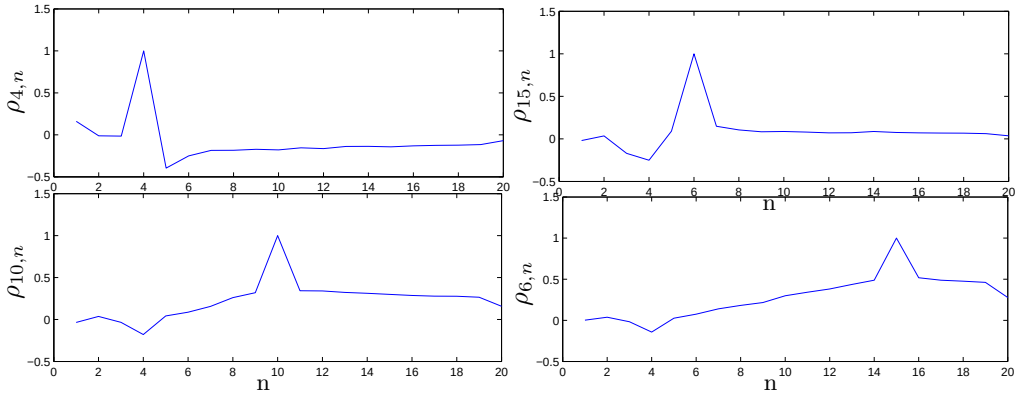

Figure 41: The figure shows the shell how the shells 4, 6, 10 and 15 are correlated to the rest of the shells

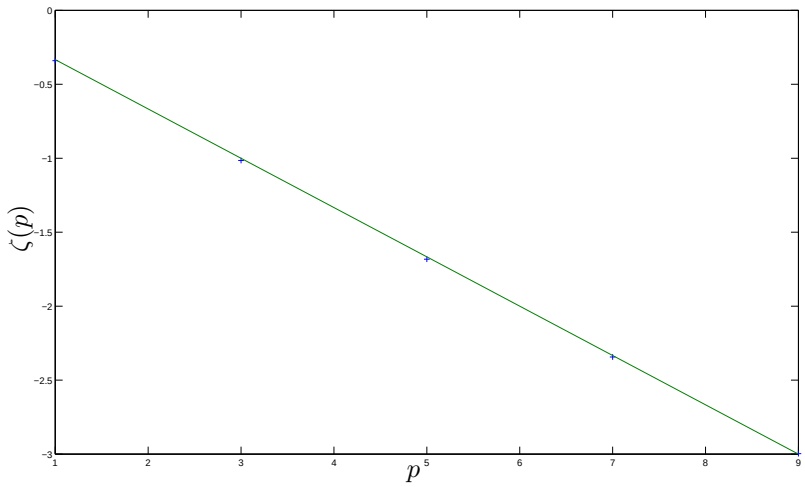

Figure 42: The figure shows the scaling exponents of the structure functions as a function of the order p of the structure functions

The characteristic correlation times(shown in the right hand figure), scale roughly with the eddy turnover time over a range of shells.

In figure 41 the correlations between different shell energies are shown. Row number 4, 6, 10 and 15 of the correlation matrix have been plotted against the shell numbers. We see that the correlations are not as local in k-space as was the case for the 2D model. The 4th shell, at which the model is forced, is negatively correlated to the rest of the shells. The rest of the shells show a tendency to be positively correlated to the shells of higher shell number. As an example, the 10th and the 18th shell have a rather large correlation of 0.23. This is quite different from the results obtained for the 2D model.

In figure 42 the scaling exponents of the structure functions estimated from the simulation ST run 6 are shown. The green line shown the K41 predictions. It is seen that the scaling exponents overlap with the K41 predictions, indicating that the 3D model does not have any intermittency corrections to the scaling exponents.

4.4 Conclusions drawn from the simulations of the 3D model

We now list the main conclusions that can be drawn from the 4 simulations of the 3D model.

All 4 simulations that have been performed show a direct cascade of energy as in the Richardson picture of turbulence, and the scaling of the energy spectrum agrees well with the K41 prediction, irrespective of the second helicity like conserved integral(determined through α). There has not been enough time to thoroughly analyse the difference in the results for the two types of triad interactions. The energy flux and spectrum does not, however, seem to differ much for the two types of triad interactions.

The analysis of the single simulation shows that characteristic correlation time for the autocorrelation functions scales approximately as the eddy turnover time in the inertial range.
It also shows that the correlations between the shells are not as local in k-space as for the 2D model. Finally, the model does not appear to have any intermittency corrections to the scaling exponents.

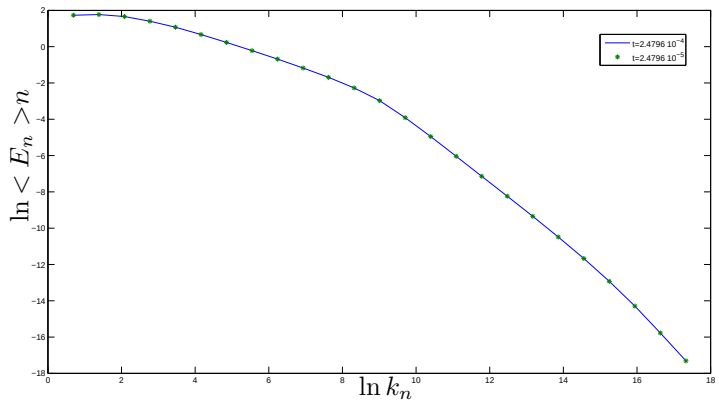

Figure 43: The figure shows two simulations of the 2D model, with the same parameters(ST run 1), but two different time steps.$\Delta t = 2.4796 \cdot 10^{-4}$(blue line) and $\Delta t = 2.4796 \cdot 10^{-5}$(green stars). The difference in shell energies between the two simulations all lie within the error on the estimates

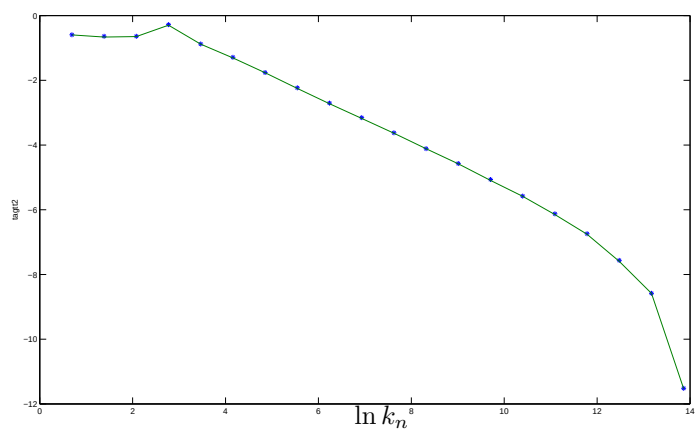

Figure 44: The figure shows two simulations of the 3D model, with the same parameters(ST run 6), but two different time steps.$\Delta t = 1.2852 \cdot 10^{-5}$(blue line) and $\Delta t = 1.2852 \cdot 10^{-6}$(green stars). The difference in shell energies between the two simulations all lie within the error on the estimates

4.5 Stability with respect to the length of the time steps

It is important that the models are stable with respect to the length of the time steps. If the models are well defined, changing the length of the time steps in a simulation, will not change the expectation values of the shell energies and the autocovariance matrix, so long as the approximations in equation 130 and 131 are still valid. The stability with respect to the length of the time steps has been tested by running simulations of the 2D model(ST run 1) and 3D model(ST run 1), with the same model parameters, but different length of the time steps. Figure 43 shows the energy spectrum for two simulations of the 2D model with the same model parameters as in ST run 1, and with the time steps $\Delta t = 2.4796 \cdot 10^{-4}$(blue line) and $\Delta t = 2.4796 \cdot 10^{-5}$(green stars). Figure 44 shows the energy spectrum for two simulations of the 3D model with the same model parameters as in ST run 6, and with the time steps $\Delta t = 1.2852 \cdot 10^{-5}$(blue line) and $\Delta t = 1.2852 \cdot 10^{-5}$(green stars). The difference in shell energies between the simulations with different time steps all lie within the error on the estimates, indicating that both the 2D and 3D model are stable with respect to the length of the time step.

5 Conclusion

The aim of the thesis project has been to develop and investigate simple stochastic cascade models of two and three dimensional turbulence, that behave in a way which resembles the behaviour of real turbulence in 2 and 3 dimensions fluids(described in section 2.2).

Such 2D and a 3D cascade models where presented in section 3. The two models are based on the idea that eddy turnovers at a certain length scale occur according to a non homogeneous Poisson process with rate parameter equal to the characteristic eddy turnover time. The eddy turnovers are constructed to redistribute the energy locally in k-space, in a way that conserves energy and helicity in the 3D model, and energy and enstrophy in 2D model. Only the local redistribution rules separate the two models, that are otherwise similar in structure.

The two models have been investigated numerically by generating realizations of the stochastic processes on a computer. The results of the simulations where presented in section 4, and show very different results for the 2D and 3D model.
The results for the 2D model agree very well with the Kraichnan double cascade picture of 2D turbulence. The model reaches a steady state where energy and enstrophy input is balanced by dissipation of energy at large length scales and dissipation of enstrophy at small length scales. When the model is forced at intermediate length scales, there is an inverse cascade of energy toward larger length scales and a direct cascade of enstrophy toward smaller length scales. In the direct cascade of enstrophy there is an inertial range where the enstrophy flux is constant and the energy spectrum scales as predicted by K41. Similarly, there is an inertial range in the inverse energy cascade where the energy flux is constant and the energy spectrum scales as predicted by K41.
The results for the 3D model agree very well with the Richardson cascade picture of 3D turbulence. The model reaches a steady state in which the energy put in to the system at large length scales is cascaded to small length scales, where it is dissipated by viscosity. There is an inertial range over which the energy flux is constant and the energy spectrum scales as predicted by K41.
An analogue to the structure functions for real turbulence has been defined for the two cascade models. One might have hoped that the models would show intermittency corrections to the scaling exponents of these structure functions, as it is seen in real turbulence. The results of the simulations show that this is not the case.

It is facinating that two simple stochastic models, as the ones presented in the thesis, can reproduce the generic features of turbulence. The two models have very different behaviours, even though they are quite similar in their structure. The only difference between the two models are the local rules for the redistribution of energy in eddy turnovers. The fact that the 2D model conserves enstrophy in the eddy turnovers, and the 3D model helicity, gives rise to such very different behaviours for the two models: A Richardson cascade for the 3D model and a Kraichnan double cascade for the 2D model

6 Dansk resumé

To simple stokastiske modeller for turbulens i en to- og tredimensionel væske er blevet presentered og undersøgt ved numeriske simulationer. De to modeller ligner hinanden i deres struktur, men har forskellige bevarede størrelser. I den friktionsløse, uforcerede grænse bevarer 2D modellen energi- og enstrofilignende størrelser, mens 3D modellen bevarer energi- og helicitetslignende størrelser.
Det er blevet vist ved numeriske simulationer at 3D modellen har en kaskade af energi mod små længdeskalaer, samt at der er et interval af længdeskalaer i hvilket energifluksen er konstant og energispektrumet skalerer som Kolmogorovs skaleringsteori forudsiger.
2D modellen, derimod, har en dobbeltkaskade: En kaskade af enstrofi mod små længdeskalaer og en kaskade af energi mod store længdeskalaer. Energispectrumet i de to kaskader stemmer overens med Kolmogorovs skaleringsteori.
Hverken 2D eller 3D modellen har intermittenskorrektioner af skaleringseksponenterne for strukturfunktionerne.

A Appendix

A.1 The index notation

In the index notation used used in the thesis it is implied that there is a summation over any index that is repeated.

$$f_i g_i = \sum_{i=1}^{i=3} f_i g_i$$

For derivatives, the notational following notations are used

$$\partial_i = \frac{\partial}{\partial x_i}$$

$$\partial_{ij} = \frac{\partial}{\partial x_i \partial x_j}$$

A.2 Newtons 2. law for a continuous material

We consider the resulting force, F_V, acting on the fluid in a volume V, bounded by the surface S. The surface forces inside the volume must balance each other, so only contributions from the bounding surface S contribute

$$F_V = \int_S \sigma_{ij}(\mathbf{x}, t) ds_i = \int_V \partial_j \sigma_{ij}(\mathbf{x}, t) dV \tag{137}$$

where Gauss theorem of integration has been used in the last step. The relation holds for any volume of fluid. If we look at a fluid particle in an infinitesimal volume dV, the velocity field will be constant over the volume, and Newtons second law for the i'th component of the motion can be written

$$\rho(\mathbf{x}, t) \frac{d^2 x_i(t)}{dt^2} dV = \rho(\mathbf{x}, t) \big[\partial_t v_i(\mathbf{x}, t) + v_j(\mathbf{x}, t) \partial_j v_i(\mathbf{x}, t)\big] dV = \partial_j \sigma_{ij}(\mathbf{x}, t) dV \tag{138}$$

Where it has been used in the second step, that the the velocity field is related to the position of the fluid particle through:

$$\mathbf{v}(\mathbf{x}, t) = \frac{d\mathbf{x}(t)}{dt}$$

A.3 Markov processes

Stochastic processes are said to posses the Markov property if their conditional probability density fulfills

$$p\big(\mathbf{x}_M, t_M \mid \mathbf{x}_{M-1}, t_{M-1};\, \mathbf{x}_{M-2}, t_{M-2};\, ...;\, \mathbf{x}_1, t_1\big) = p\big(\mathbf{x}_M, t_M \mid \mathbf{x}_{M-1}, t_{M-1}\big) \tag{139}$$

Where $[t_1, t_2, ..., t_M]$ is a set of growing times and

$$p\big(\mathbf{x}_M, t_M \mid \mathbf{x}_{M-1}, t_{M-1};\, \mathbf{x}_{M-2}, t_{M-2};\, ...;\, \mathbf{x}_1, t_1\big)\mathrm{d}\mathbf{x} \tag{140}$$

is the probability that the random variable at time t_M has outcome in the hyper cube $[\mathbf{x_M}, \mathbf{x_M} + d\mathbf{x}]$, given that the random variable at earlier times had the outcomes $\{\hat{X}(t_{m-1}) = x_{M-1}, \hat{X}(t_{M-2}) = x_{M-2}, ..., \hat{X}(t_1) = x_1\}$.
Such a process is forgetful, in the sense that the probability density of one random variable in the sequence, only depends on the outcome of the previous random variable.

References

Ditlevsen, P. (2004), *Turbulence and Climate Dynamics*, Frydenberg, Copenhagen.

Ditlevsen, P. D., and I. A. Mogensen (1996), Cascades and statistical equilibrium in shell models of turbulence, *Phys. Rev. E*, *53*(5), 4785–4793, doi:10.1103/PhysRevE.53.4785.

F. Anselmet, E. J. H., Y. Gagne, and R. A. Antonia (1984), High-order velocity structure functions in turbulent shear flows, *journal of fluid mechanics*, *140*.

Frisch, U. (1995), *Turbulence*, Cambridge, UK.

Wang, C. (1990), Exact solutions of the navier-stokes equations-the generalized beltrami flows, review and extension, *Acta Mechanica*, *81*, 69–74, 10.1007/BF01174556.

Yamada, M., and K. Ohkitani (1987), Lyapunov spectrum of a chaotic model of three-dimensional turbulence, *Journal of the Physical Society of Japan*, *56*(12), 4210–4213, doi: 10.1143/JPSJ.56.4210.

List of Figures

List of Tables